ELSEVIER

Biochemical Pharmacology 62 (2001) 829–851

Biochemical Pharmacology

Apparent capacity of cardiac muscarinic receptors for different radiolabeled antagonists

Chi Shing Sum, Norman Pyo, James W. Wells*

Department of Pharmacology and Faculty of Pharmacy, University of Toronto, 19 Russell St., Toronto, Ontario, Canada M5S 2S2

Received 5 September 2000; accepted 2 January 2001

Abstract

Muscarinic receptors in sarcolemmal membranes, digitonin-solubilized extracts, and purified preparations from porcine atria have revealed a shortfall in the apparent capacity for *N*-[^{3}H]methylscopolamine, which was only about 75% of that for [^{3}H]quinuclidinylbenzilate. Since binding at near-saturating concentrations of [^{3}H]quinuclidinylbenzilate was inhibited fully at comparatively low concentrations of unlabeled *N*-methylscopolamine, the data are inconsistent with the notion that [^{3}H]quinuclidinylbenzilate binds selectively to a subclass of distinct, non-interconverting, and mutually independent sites. The discrepancy is resolved by adjusting the specific activity of *N*-[^{3}H] methylscopolamine to account for unlabeled scopolamine that was identified in some batches of the radioligand. Also, there was no shortfall in capacity when *N*-[^{3}H]methylscopolamine was devoid of scopolamine, and the predicted effect was obtained when pure *N*-[^{3}H]methylscopolamine was supplemented with known amounts of scopolamine. A small discrepancy in the levels of scopolamine estimated pharmacologically and by mass spectrometry can be attributed largely to a difference in the efficiency of ionization between scopolamine and *N*-methylscopolamine. Different capacities for different radioligands are not uncommon with muscarinic and other G protein-coupled receptors, and in some cases the effect may have been due wholly or in part to an unlabeled impurity. Binding data can be mechanistically ambiguous, particularly when acquired only at graded concentrations of the radioligand. The predicted effects of an unlabeled impurity mimic or resemble those of alternative scenarios such as sequestration behind a hydrophobic barrier, a nucleotide-regulated interconversion from one state of affinity to another, and cooperativity between interacting sites.

Keywords: Binding parameters; Radioligands; Muscarinic receptors; Artifacts

1. Introduction

Compounds radiolabeled to a high specific activity are uniquely suited for studies on the binding properties of receptors and other macromolecules. Their high sensitivity permits measurements at very low levels of labeled material, extending to attomole quantities in the case of some nuclides. Also, the measured signal depends only on the specific radioactivity and the efficiency of the counting process. The former is known in advance, at least in principle, and the latter usually can be measured to a high degree of precision. Since the specific signal is invariant, the amount of labeled compound can be determined readily in absolute units.

Tritium is a particularly useful nuclide owing to its comparatively long half-life and its specific activity of 28.8 Ci/matom, which is well matched to the levels of receptor found in many preparations. Isotopic purity approaches 100% in many commercial products, and the substitution of tritium for hydrogen generally appears to have little or no discernible effect on the properties of the ligand. This equivalence is often assumed, but in many cases it can be tested by comparing the binding of the radioligand with that of the unlabeled analogue. The synthesis of tritiated compounds generally yields a mixture of two or more products differing in the distribution of tritium and hydrogen atoms within the molecule. Since the labeled and unlabeled compounds are pharmacologically indistinguishable, the effective specific activity can be calculated as a weighted average based on the specific activities and relative amounts of the different species.

The binding pattern defined by graded concentrations of

* Corresponding author. Tel.: +1-416-978-3068; fax: +1-416-978-8511.

E-mail address: jwells@phm.utoronto.ca (J.W. Wells).

Abbreviations: ABT, 3-(2′-aminobenzhydryloxy)tropane; ECL, enhanced chemiluminescence; NMS, *N*-methylscopolamine; PMSF, phenylmethylsulfonyl fluoride; and QNB, *l*-quinuclidinylbenzilate.

0006-2952/01/$ – see front matter
PII: S0006-2952(01)00726-2

a radioligand at thermodynamic equilibrium is sensitive to radiochemical and chemical impurities [1–5]. While the radiochemical purity typically is stated by the manufacturer, chemical purity tends to have a lower profile. It has been pointed out, however, that disregarding an unlabeled contaminant is akin to overestimating the specific activity of the radioligand [3–5]. The concentration of the radioligand therefore is underestimated throughout, and that, in turn, leads to artifactually low values of both the capacity and the potency (i.e. EC_{50}) in a population of identical and mutually independent sites.

In studies on cardiac muscarinic receptors, batches of the muscarinic antagonist *N*-[^{3}H]methylscopolamine were found to contain appreciable quantities of the unlabeled precursor scopolamine; similarly, batches of *N*-[^{3}H]methylquinuclidinylbenzilate were found to contain unlabeled quinuclidinylbenzilate. In the present report, we compare the binding of contaminated *N*-[^{3}H]methylscopolamine, *N*-[^{3}H]methylscopolamine devoid of scopolamine, and [^{3}H]quinuclidinylbenzilate to muscarinic receptors from porcine atria. A competition between *N*-[^{3}H]methylscopolamine and contaminating scopolamine can account for results that otherwise are anomalous in terms of mutually independent sites. Possible alternatives to the notion of a contaminated radioligand are considered and, in some cases, ruled out. Strategies are employed to estimate the amount of the impurity and to determine the effective specific activity of an impure product according to a model that seems to fit. The results suggest that chemical impurities have contributed to various effects used routinely to monitor the properties of muscarinic and other G protein-linked receptors. A preliminary report of this work has appeared elsewhere [6].

2. Materials and methods

2.1. Muscarinic ligands

N-[^{3}H]Methylscopolamine was obtained as the chloride salt from NEN Life Science Products, Inc. (lot 2924211, 84.0 Ci/mmol; lot 3144205, 84 Ci/mmol; lot 3167197, 84.5 Ci/mmol; lot 3318049, 82.0 Ci/mmol; lot 3273247, 82.0 Ci/mmol; lot 3406009, 83.5 Ci/mmol) and as the bromide salt from Amersham Pharmacia Biotech (batch 27, 78.3 Ci/mmol). *N*-[^{3}H]Methylquinuclidinylbenzilate was obtained as the chloride salt from NEN (lot 3248957, 83.5 Ci/mmol; lot 3329162, 83.5 Ci/mmol; lot 3329351, 83.5 Ci/mmol; lot 3329582, 84.0 Ci/mmol; lot 3329817, 84.0 Ci/mmol; lot 3363021, 82.0 Ci/mmol; lot 3363297, 81.0 Ci/mmol). (−)-[^{3}H]Quinuclidinylbenzilate was obtained from NEN (lot 2824273, 43.5 Ci/mmol; lot 3186289, 52.3 Ci/mmol; lot 3231205, 43.5 Ci/mmol; lot 3329039, 49.0 Ci/mmol; lot 3329907, 42.0 Ci/mmol) and from Amersham (batch 44, 48 Ci/mmol).

All radioligands were used as supplied by the manufacturer. The *N*-[^{3}H]methylscopolamine obtained from Amersham had been purified by paper chromatography; that from NEN had been purified by HPLC (lot 3406009) or by paper chromatography (all other lots). The absence of scopolamine from *N*-[^{3}H]methylscopolamine supplied by Amersham was indicated by a mass spectrum provided by the manufacturer. In the case of *N*-[^{3}H]methylscopolamine from NEN, mass spectra for four lots were available from the manufacturer or were obtained at the University of Toronto (UT). The molar ratio of scopolamine to *N*-[^{3}H]methylscopolamine was estimated from peak height (NEN, UT) or area (UT), and the values are as follows: lot 3167197, 1.2 (NEN); lot 3318049, 0.86 (NEN); lot 3273247, 0.74 (UT, peak height), 0.76 (UT, peak area); lot 3406009, nil (NEN, UT). The absence of scopolamine from lot 3406009 was confirmed by thin-layer chromatography carried out by the manufacturer.

Unlabeled *N*-methylscopolamine hydrobromide was purchased from Sigma-Aldrich. Scopolamine hydrobromide was purchased as the dihydrate from RBI-Sigma, and the hydration state was confirmed by elemental analysis (Canadian Microanalytical Service, Ltd.). The measured composition is as follows: C, 49.86%; H, 5.97%; N, 3.40%; O, 21.91%. The calculated composition for different states of hydration (in percent) is as follows: anhydrous—C, 53.14; H, 5.77; N, 3.65; O, 16.65; $1H_2O$—C, 50.76; H, 6.01; N, 3.48; O, 19.89; $2H_2O$—C, 48.58; H, 6.24; N, 3.33; O, 22.84; $3H_2O$—C, 46.58; H, 6.44; N, 3.20; O, 25.55; $4H_2O$—C, 44.74; H, 6.63; N, 3.07; O, 28.05.

2.2. Detergents, antisera, and other materials

Digitonin generally was obtained from Wako Bioproducts at a purity of nearly 100%; material of lower purity was obtained on occasion from Roche Diagnostics (>75%, 93%), ICN Biomedicals (50%), and Sigma-Aldrich (50%). The latter products were used primarily to elute the columns of Sephadex G-50 during the binding assays, but there was no discernible difference when they were used in place of the product from Wako to solubilize the receptor. Sodium cholate was purchased from Sigma-Aldrich.

HEPES was obtained as the free acid from Roche Diagnostics. EDTA was obtained as the free acid from British Drug Houses or as the disodium salt from Bioshop Canada Inc. Dithiothreitol, bacitracin, all protease inhibitors, trimethylchlorosilane, Tween-20, and Sephadex G-50 (fine) were from Sigma-Aldrich. Protein was estimated by the Lowry method; the reagents and bovine serum albumin, taken as the standard, were purchased from Pierce.

Antisera were from the same sources as reported previously [7]. Ascites fluid containing a monoclonal antibody to the porcine M_2 muscarinic receptor was obtained initially as a gift from Dr. Neil M. Nathanson, Department of Pharmacology, University of Washington (31–1D1), and later batches were purchased from Affinity Bioreagents. Reagents and film for recording chemiluminescence from

western blots were purchased from Amersham (ECL™, Hyperfilm MP) or NEN Life Science Products (Reflection).

ABT-Sepharose used in the purification of m2 receptor was prepared essentially as described previously [7]; epoxy-activated Sepharose 6B and FastFlow DEAE-Sepharose were from Amersham Pharmacia Biotech. Econo-Pac HTP (CHT-II) and Econo-Pac P6 cartridges were purchased from Bio-Rad Laboratories. Solubilized and purified receptor was concentrated as required by means of Centricon-10 and Centriprep-30 filters (Amicon) purchased from the Millipore Corp.

2.3. Mass spectrometry

Spectra were obtained at the Mass Spectrometry Laboratory, Molecular Medicine Research Centre, University of Toronto, using a Sciex API III+ spectrometer (Perkin-Elmer) operated in the ion spray mode. The spectrum of *N*-[^{3}H]methylscopolamine was obtained as a full scan from *m*/*z* 152 to *m*/*z* 600. Scopolamine and unlabeled *N*-methylscopolamine were characterized by full scan and by selective ion monitoring at *m*/*z* 304 and *m*/*z* 318. Mass spectra provided by NEN Life Science Products, Inc. were obtained by fast atom bombardment.

2.4. Preparations of m2 muscarinic receptor

Purified m2 receptor solubilized in digitonin-cholate (0.1% digitonin, 0.02% sodium cholate) was prepared from porcine atria via affinity chromatography on ABT-Sepharose as described previously [7]. Early experiments were performed on the eluant from an Econo-Pac P6 cartridge [i.e. preparation M2 in Ref. 7), which was stored on ice until required for the binding assays. For later experiments, passage of sample through the Bio-Gel P6 was omitted; rather, the eluate from an Econo-Pac HTP cartridge was concentrated from 6 mL to about 0.5 mL (Centricon-10), diluted to 2 mL with buffer D[1] supplemented with 0.1% digitonin and 0.02% sodium cholate, and then stored in aliquots (20–60 μL) at –75°. Frozen samples were thawed, diluted 15- to 25-fold with buffer E supplemented with 0.1% digitonin and 0.02% sodium cholate, and stored on ice for 24 hr prior to the binding assays. These changes were without effect on the binding of *N*-[^{3}H]methylscopolamine or [^{3}H]quinuclidinylbenzilate. Purified receptor was shown by western blotting to be devoid of the alpha subunits of G_o, G_{i1}, G_{i2}, $G_{q/11}$, and G_s. The sucrose gradient typically yielded 90–120 mg of protein from about 350 g of left plus right atria.

For binding assays on solubilized extracts, the sarcolemmal fraction from the sucrose gradient [7] was diluted 6–10-fold with ice-cold buffer A and centrifuged for 40 min at 4° and 100,000 *g* (Beckman, 45Ti). The pellets were resuspended in a small volume of buffer D (Brinkmann Polytron, setting 5, 10 sec), diluted 12-fold with the same buffer, and centrifuged as before. This step was repeated at a dilution of 20–22-fold in buffer D, and the pellets were stored at −75°. Each pellet contained the material for one preparation of solubilized receptor, which was sufficient for several binding experiments. To extract the receptor, the pellet was thawed on ice and resuspended in ice-cold buffer D (5.5 mg of protein per mL). Nine volumes of the suspension then were mixed with 1 volume of a stock solution containing 4% digitonin (Wako) and 0.8% sodium cholate in buffer D. Solubilization was carried out according to the two-step procedure of Peterson and Schimerlik [8], as in the preparation of purified receptor [7], except that buffer D was substituted for the imidazole-containing buffer used previously (cf. buffer D in footnote 1 and buffer A in Ref. 7). The solubilized receptor was stored on ice until required in the binding assays.

For binding assays on sarcolemmal membranes, the material collected from the sucrose gradient was diluted at least 3-fold with ice-cold buffer B and centrifuged for 40 min at 4° and 100,000 *g*. The pellets were resuspended in a small volume of buffer B (Polytron, setting 5, 10 sec), diluted 20- to 25-fold with the same buffer, and divided into aliquots containing sufficient material for one experiment. The aliquots were centrifuged for 40 min at 4° and 150,000 *g*, and the pellets were stored at –75°.

2.5. Binding assays

For binding to solubilized receptor, 50 μL of a solution containing all of the ligands in buffer E supplemented with 0.1% digitonin and 0.02% sodium cholate was added to 3 μL of the solubilized preparation in polypropylene microcentrifuge tubes pretreated with trimethylchlorosilane. The reaction mixture was incubated for 45 min in assays with *N*-[^{3}H]methylscopolamine or for 2 hr in assays with [^{3}H]quinuclidinylbenzilate. The temperature of incubation was 30° throughout. The reaction was terminated, and the bound radioligand was separated by applying an aliquot of the sample (50 μL) to a column of Sephadex G-50 fine (0.3 × 6.5 cm) pre-equilibrated and eluted with buffer E supplemented with 0.017% digitonin. All of the eluant up to and including the void volume was collected (1.45 mL) and assayed for radioactivity.

For binding to sarcolemmal membranes, frozen pellets

[1] Buffer solutions are abbreviated as follows: buffer A [7], 20 mM imidazole, 1 mM EDTA, 0.1 mM PMSF, 0.02% (w/v) sodium azide, 1 mM benzamidine, 2 μg/mL of pepstatin A, 0.2 μg/mL of leupeptin, 200 μg/mL of bacitracin, pH 7.60 with HCl; buffer B, 20 mM HEPES, 1 mM EDTA, 200 μg/mL of bacitracin, pH 8.0 with KOH; buffer C, 50 mM HEPES, 1 mM $MgCl_2$, pH 7.45 with KOH; buffer D, 20 mM KH_2PO_4, 20 mM NaCl, 1 mM EDTA, 0.1 mM PMSF, pH 7.40 with KOH; buffer E, 20 mM HEPES, 1 mM EDTA, 20 mM NaCl, 5 mM $MgSO_4$, 0.1 mM PMSF, pH 7.40 with NaOH. Buffers A–C and E were obtained by dilution of a stock solution prepared at the desired pH and at 10-fold the final concentration; protease inhibitors were added to the diluted solution as required. Buffer D was prepared from stock solutions of KH_2PO_4, EDTA, and NaCl adjusted to the desired pH with KOH (for KH_2PO_4) or NaOH (for EDTA); PMSF was added to the diluted solution. All solutions were titrated to the desired pH at room temperature.

containing 8–10 mg of protein and prepared in buffer B were thawed on ice and suspended in 5–6 mL of buffer C (Polytron, setting 5, 10 sec). Following the Lowry assay, the homogenate was diluted with buffer C to yield a final protein concentration of 0.1 g/L. Aliquots of this suspension (490 μL) were added to polypropylene microcentrifuge tubes containing the radioligand and any other ligands dissolved in deionized water (10 μL) at 50 times the final concentration. The reaction mixture was incubated for 1 hr in assays with *N*-[^{3}H]methylscopolamine and for 2 hr in assays with [^{3}H]quinuclidinylbenzilate. The temperature of incubation was 30° throughout, and bound radioligand was separated by microcentrifugation at 12,000 *g* for 5 min (Beckman, Microfuge 12).

For both membrane-bound and solubilized receptors, it was confirmed that the period of incubation was sufficient for binding to become independent of time. The binding profile defined by *N*-[^{3}H]methylscopolamine was found to be superimposable after incubation of the samples for up to 2.4 hr; similarly, the binding profile defined by [^{3}H]quinuclidinylbenzilate was the same after incubation for up to 5 hr. The apparent capacity for *N*-[^{3}H]methylscopolamine and [^{3}H]quinuclidinylbenzilate was compared throughout in assays with both radioligands taken in parallel. Non-specific binding increased linearly with the concentration of either radioligand and was taken as total binding in the presence of 0.1 or 1 mM unlabeled *N*-methylscopolamine. The non-specific binding of [^{3}H]quinuclidinylbenzilate to sarcolemmal membranes was comparatively high, representing about 2% of the unbound ligand; nonetheless, the line of demarcation between specific and non-specific binding was the same regardless of whether the latter was defined by 1 mM *N*-methylscopolamine or 10 μM quinuclidinylbenzilate. In solubilized preparations, non-specific binding represented less than 0.06% of unbound [^{3}H]quinuclidinylbenzilate and 0.005% of unbound *N*-[^{3}H]methylscopolamine.

Assays were carried out in duplicate or triplicate for preparations in digitonin-cholate and in quadruplicate for membranes. Each sample was counted twice by liquid scintillation spectrometry (Beckman LS7800, Beckman LS5000, or Packard 2100TR), and the individual values were averaged to obtain the mean and standard error used in subsequent analyses. Absolute count rates were determined by means of an external standard. Additional details regarding the binding assays have been described elsewhere [7,9, 10].

2.6. Analysis of data

All data were analyzed according to Eq. 1, in which B_{obsd} and B_{sp} represent total observed binding and specific binding, respectively. The parameter *NS* represents the fraction of unbound radioligand (i.e. $[P] = [P]_t - B_{sp}$) that appears as non-specific binding, which was found to increase linearly with [P] for both antagonists under all conditions. Subsequent manipulations of the data were for the purpose of presentation only and did not alter the relationship between the data and the fitted curve.

$$B_{obsd} = B_{sp} + NS([P]_t - B_{sp}) \quad (1)$$

For data acquired at graded concentrations of the radioligand, the value of B_{sp} in Eq. 1 was calculated empirically according to Eq. 2; the parameter n_H represents the Hill coefficient, and $[P]_t$ represents the total concentration of [^{3}H]quinuclidinylbenzilate or *N*-[^{3}H]methylscopolamine. The parameter B_{max} represents maximal specific binding, and EC_{50} represents the concentration of unbound radioligand when B_{sp} equals $1/2B_{max}$. Equation 2 was solved numerically in the manner described previously (cf. Eq. 204 in Ref. 11).

$$B_{sp} = B_{max}\frac{([P]_t - B_{sp})^{n_H}}{EC_{50}^{n_H} + ([P]_t - B_{sp})^{n_H}} \quad (2)$$

Mechanistic descriptions of the data were based on Scheme 1, in which *m* ligands (i.e. L_i, $i = 1, m$) compete for a heterogeneous mixture of distinct, non-interconverting, and mutually independent sites (i.e. R_j, $j = 1, n$). The affinity of each L_i for the sites of class *j* is represented by the equilibrium dissociation constant (i.e. $K_{ij} = [L_i][R_j]/[L_iR_j]$).[2] The radioligand is shown as L_k in Eqs. 3–5 (i.e. $i = k$) and as L_1 in Eq. 6 (i.e. $i = 1$); the labeled complex with each R_j is therefore L_kR_j and L_1R_j, respectively, and the corresponding dissociation constants are K_{kj} and K_{1j}.

$$L_i + R_j \underset{}{\overset{K_{ij}}{\rightleftharpoons}} L_iR_j$$

Scheme 1

The value of B_{sp} in Eq. 1 was calculated according to Eq. 3. Quinuclidinylbenzilate, *N*-methylscopolamine, and scopolamine were designated as ligands 1, 2, and 3, respectively, and the value of *k* therefore depends upon whether [^{3}H]quinuclidinylbenzilate or *N*-[^{3}H]methylscopolamine was selected as the radioligand. Capacity was formulated as the total concentration of all sites (i.e. $[R]_t = \Sigma_{j=1}^{n}[R_j]_t$) and the fraction thereof corresponding to those of each class (i.e. $F_j = [R_j]_t/[R]_t$). The parameter f_R is a scaling factor that was used to obtain estimates of the relative capacity between two or more sets of data. When *N*-[^{3}H]methylscopolamine and [^{3}H]quinuclidinylbenzilate were assayed in parallel, the capacity for the former generally was estimated relative to that for the latter. The values of B_{sp}, B_{max}, and $[R]_t$ are shown throughout as the concentration in the binding assay (pM).

[2] Comparatively low values of K_{ij} are referred to as high affinity, and higher values of K_{ij} are referred to as low affinity. Similarly, statements of high or low potency are with reference to the value of $1/EC_{50}$.

$$B_{sp} = \sum_{j=1}^{n} [L_k R_j]$$

$$\equiv f_R[R]_t \sum_{j=1}^{n} \frac{F_j[L_k]}{[L_k] + K_{kj}\left(1 + \sum_{\substack{i=1 \\ i\neq k}}^{m} \frac{[L_i]}{K_{ij}}\right)}$$

$$\equiv f_R[R]_t \sum_{j=1}^{n} \frac{F_j \frac{[L_k]}{K_{kj}}}{1 + \sum_{i=1}^{m} \frac{[L_i]}{K_{ij}}} \quad (3)$$

In most experiments, binding led to an appreciable reduction in the concentration of unbound radioligand under at least some conditions. The values of $[L_i]$ required by Eq. 3 therefore were computed throughout from the corresponding implicit equations for $[L_i]_t$ (i.e. $[L_i] + \Sigma_{j=1}^{n}[L_i R_j] - [L_i]_t = 0$, where $i = 1, m$). Thus, the values plotted on the x-axis in Figs. 2–5 denote the total molar concentration in the binding assay. The system of m implicit equations was solved numerically as described previously [11].

In some analyses, the total concentration of an unlabeled ligand i was entered explicitly as an independent variable. In others, the value was calculated as the constant fraction f_i of the total concentration of L_k (Eq. 4). This arrangement permits f_i to be treated as a parameter, which then can be optimized as required.

$$f_i = \frac{[L_i]_t}{[L_k]_t} \quad (4)$$

2.7. Simulations

Data were simulated with respect to the free concentrations of all ligands, and depletion therefore was assumed to be negligible. For simulations in terms of Scheme 1, the parameter f_i was introduced by substituting $f_i[L_k]$ for $[L_i]$ in Eq. 3 to obtain Eq. 5 ($f_i = 1$ when $i = k$). The definition of f_i is strictly correct only for total concentrations, but it also will apply to free concentrations if neither ligand is depleted through binding to the receptor. The implications of Eq. 5 are considered further in the Appendix.

$$B_{sp} = \sum_{j=1}^{n} [L_k R_j]$$

$$\equiv f_R[R]_t \sum_{j=1}^{n} \frac{F_j[L_k]}{[L_k] + K_{kj}\left(1 + [L_k] \sum_{\substack{i=1 \\ i\neq k}}^{m} \frac{f_i}{K_{ij}}\right)}$$

$$\equiv f_R[R]_t \sum_{j=1}^{n} \frac{F_j \frac{[L_k]}{K_{kj}}}{1 + [L_k] \sum_{i=1}^{m} \frac{f_i}{K_{ij}}} \quad (5)$$

Eq. 5 can be rearranged as in Eq. A1 or A2 of the Appendix, taking f_R as 1 and substituting $[R_j]_t$ for $F_j[R]_t$. The resulting expression can be simplified to one class of sites ($n = 1$) and two ligands ($m = 2$) as in Eq. 6, where L_1 is the probe and L_2 is a contaminant ($f_2 = [L_2]/[L_1]$). Equation 6 is analogous to Eq. 3 or 4 in Ref. 4.

$$B_{sp} = [L_1 R] \equiv \frac{\frac{[R]_t}{\left(1 + f_2 \frac{K_1}{K_2}\right)}[L_1]}{\frac{K_1}{\left(1 + f_2 \frac{K_1}{K_2}\right)} + [L_1]} \quad (6)$$

Data also were simulated according to Scheme 2, in which a tetravalent and presumably tetrameric receptor (R) can bind up to four equivalents of a radioligand (P).

$$R \underset{}{\overset{[P]}{\rightleftharpoons}} P_1R \overset{[P]}{\rightleftharpoons} P_2R \overset{[P]}{\rightleftharpoons} P_3R \overset{[P]}{\rightleftharpoons} P_4R$$

$$\frac{[P]\,[R]}{[P_1R]} = K_P \qquad \frac{[P]\,[P_{j-1}R]}{[P_jR]} = \prod_{i=2}^{j} p_i K_P$$

Scheme 2

The parameter K_P is the microscopic dissociation constant for the binding of P to any site on the vacant receptor, and p_j is the cooperativity factor for binding of the jth equivalent of P to form P_jR. The system therefore exhibits positive cooperativity when p_j is less than 1 and negative cooperativity when p_j exceeds 1. While a multivalent receptor could be both cooperative and asymmetric, each asymmetric arrangement has a symmetric equivalent when the specific signal from the ligand is invariant. It therefore is assumed here that all vacant sites are equivalent at each level of occupancy.

Specific binding was calculated according to Eq. 7, where each coefficient is the product of the degree of occupancy (i.e. 1–4) times the number of positional isomers. The values of $[P_jR]$ were calculated from the expansions in terms of $[R]_t$ and [P]. Further details regarding the formulation of cooperative models have been described elsewhere [11].

$$B_{sp} = 4[P_1R] + 12[P_2R] + 12[P_3R] + 4[P_4R] \quad (7)$$

2.8. Plotting and statistical procedures

The results of analyses involving multiple sets of data from replicated experiments have been presented throughout with reference to a single fitted curve. To obtain the

values plotted on the y-axis, estimates of B_{obsd} were adjusted according to the expression $B'_{obsd} = B_{obsd}\ \{f(\bar{\mathbf{x}}_i, \bar{\mathbf{a}})/f(\mathbf{x}_i, \mathbf{a})\}$. The function f represents the fitted model. The vectors $\mathbf{x}_i$ and $\mathbf{a}$ represent the independent variables at point i and the fitted parameters for the set of data under consideration; $\bar{\mathbf{x}}_i$ and $\bar{\mathbf{a}}$ are the corresponding vectors in which values that differ from experiment to experiment have been replaced by the means for experiments associated with the fitted curve. Individual values of B'_{obsd} at the same $\mathbf{x}_i$ were averaged to obtain the mean and standard error plotted in the figure. The y-axis represents specific binding (B_{sp}) throughout: that is, the value of B'_{obsd} less the fitted estimate of non-specific binding at the same concentration of unbound radioligand [12].

All parameters were estimated by non-linear regression, and values at successive iterations of the fitting procedure were adjusted according to the algorithm of Marquardt [13]. Affinities were optimized on a logarithmic scale (i.e. log K_{ij}). Most analyses involved multiple sets of data, and specific details regarding the assignment of shared parameters are described where appropriate. Values of $[R]_t$ were assigned separately to data from separate experiments; values of *NS* generally were common to all data acquired with the same radioligand in the same experiment.

Weighting of the data, tests for significance, and other statistical procedures were performed as described elsewhere [11,14]. Weighted residuals were of comparable magnitude within each set of data. In simultaneous analyses, individual sets of data generally made comparable contributions to the total weighted sum of squares; thus, the fits were not dominated by the data from one experiment or group of experiments. Mean values calculated from two or more individual estimates of a parameter or other quantity are presented together with the standard error. For parametric values derived from a single analysis of one or more sets of data, the errors were estimated from the diagonal elements of the covariance matrix. Such values reflect the range within which the weighted sum of squares is essentially the same.

3. Results

Data on the binding properties of G protein-linked receptors typically are analyzed in terms of Scheme 1, either implicitly as a sum of hyperbolic terms or explicitly according to Eq. 3 or equivalent expressions. In studies at graded concentrations of the radioligand, designated below as L_1, unlabeled compounds generally are assumed to be absent except when added to define the level of non-specific binding (i.e. $[L_i]/K_{ij} \gg [L_1]/K_{1j}$).

If non-radiolabeled ligands are present, their effect depends upon whether or not they constitute an additional variable within the system. When present at a constant concentration, they act to reduce the apparent affinity of the radioligand without affecting the estimate of $[R]_t$ (e.g. Eq. 3). The effects are more complex when the concentration varies, but a special case arises when a non-radiolabeled impurity is present with the radioligand. With two ligands and one class of sites, the effect of an unlabeled contaminant is to reduce both the apparent capacity and the apparent affinity by the factor $1+f_2K_1/K_2$ (Eq. 6). The analogous effect expected with multiple ligands and multiple classes of sites is described in the Appendix (Eq. A2).

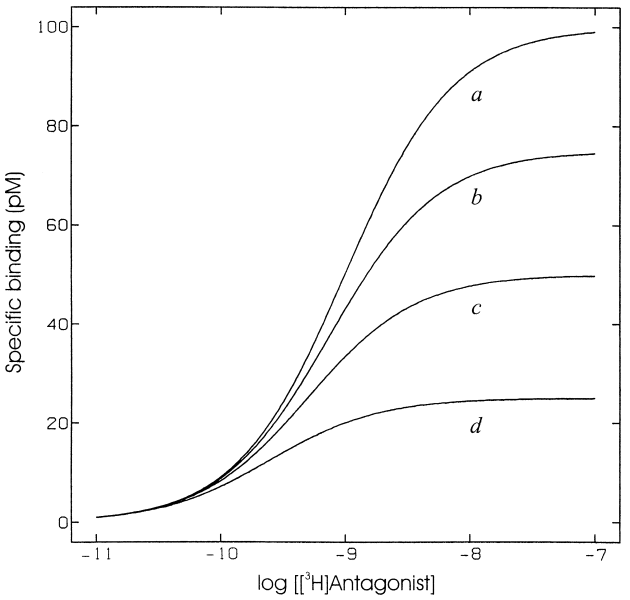

Fig. 1. Equivalent binding profiles predicted for chemically pure and impure radioligands under different mechanistic assumptions. The lines shown in the figure can be simulated using any of the schemes and corresponding parametric values listed in Table 1. Binding was calculated with respect to the free concentration of the radioligand, and all of the lines conform to a rectangular hyperbola.

The effect of a contaminant on the binding profile defined by graded concentrations of a probe is illustrated in Fig. 1, where the lines can be computed according to Scheme 1 (Eq. 6) or alternative models as described in the Discussion. The simulations illustrate four different scenarios in which the maximal binding is 100, 75, 50, or 25 pM, and the parametric values are listed in Table 1. The magnitude of the effect of the contaminant on B_{max} depends upon its affinity relative to that of the probe (i.e. K_1/K_2 in Eq. 6). When the affinity of the probe is comparatively high (e.g. $K_1 = 10^{-9}$, $K_2 = 10^{-8}$, $K_1/K_2 = 0.1$), a 3-fold molar excess of the contaminant is required to reduce the apparent capacity by 25% ($f_2 = 3.3$); an equimolar amount of the contaminant would reduce the apparent capacity by only 9% ($f_2 = 1$). When the affinity of the probe is comparatively weak (e.g. $K_1 = 10^{-9}$, $K_2 = 10^{-10}$, $K_1/K_2 = 10$), the apparent capacity is reduced by 25% when the concentration of the contaminant is only 3% of that of the probe. Parallel changes emerge in the potency of the probe, since the effective concentration of ligand is consistently underestimated owing to the presence of the contaminant.

As described in the Appendix, the effect of the unlabeled

Table 1
Conditions for equivalent effects from different mechanistic proposals

	Langmuir isotherm[a]		Scheme 1 ($n = 1$)[b]				Scheme 1 ($n = 4$)[c]				Scheme 2[d]			
				f_2										
Curve	log EC_{50}	B_{max} (pM)	log K_1	log K_2 = −10	log K_2 = −9	log K_2 = −8	i	log K_{1i}	l	log K_{1l}	log K_P	log p_2	log p_3	log p_4
a	−9.00	100	−9.00	0.0	0.0	0.0	1–4	−9.00			−9.00	0.0	0.0	0.0
b	−9.13	75	−9.00	0.033	0.33	3.3	1–3	−9.13	4	>−5	−9.00	0.051	0.12	>4.0
c	−9.30	50	−9.00	0.10	1.0	10	1–2	−9.30	3–4	>−5	−9.00	0.18	>4.0	
d	−9.60	25	−9.00	0.30	3.0	30	1	−9.60	2–4	>−5	−9.00	>4.0		

For each model, the values listed in the table correspond to curves *a–d* in Fig. 1. Binding was calculated with respect to the free concentrations of all ligands in Schemes 1 and 2. The value of $[R]_t$ is 100 pM in Scheme 1 and 25 pM in Scheme 2.

[a] $B_{obsd} = B_{max}\,[L_1]/(EC_{50} + [L_1])$.

[b] Binding to a homogeneous population of sites when a non-radiolabeled impurity (L_2) is present in constant molar ratio (f_2) relative to the radioligand (L_1) (Eq. 6). Three examples are shown, differing in K_2. The net effect of the impurity is determined by the product of f_2 and the ratio K_1/K_2.

[c] Binding to a heterogeneous population comprising four, equally populated classes of mutually independent sites (i.e. $F_j = 1/n$ for all j) (Eq. 3, $k = 1$, $m = 1$). The sites of each class are of either high affinity (K_{1i}) or unobservably low affinity (K_{1l}) for the radioligand (L_1).

[d] Binding to a tetravalent receptor (Eq. 7) when saturation is precluded by negative cooperativity (i.e. $p_j > 10^4$). The parameters were selected to yield binding profiles congruent with those simulated according to Scheme 1, and each curve therefore has a Hill coefficient of 1. Owing to the difference between macroscopic and microscopic affinity at each level of occupancy, the cooperativity factors p_2 and p_3 are not 1 when B_{max} is either 0.75 (curve *b*) or 0.50 (curve *c*). Scheme 2 is described by a fourth degree Adair equation with respect to $[L_1]$, as is Scheme 1 under the conditions described in footnote "*c*" above (i.e. $[R_j]_t = \frac{1}{4}[R]_t$ for all j) [11].

ligand can be subsumed in an appropriate value of the specific radioactivity. Curves *b–d* in Fig. 1 would be superimposable with curve *a* if the specific activity of the probe were reduced in each case by the factor $1/(1+f_2K_1/K_2)$ (i.e. 0.75, 0.50, and 0.25 for curves *b–d*, respectively). Such a correction is valid only for the particular conditions of the experiment, since any change might affect the value of K_1/K_2. In that event, the effective specific activity would change accordingly, with parallel changes in the position and amplitude of the binding curve (e.g. EC_{50} and B_{max} in Eq. 2). If the ratio of affinities were unfavorable (i.e. $K_1/K_2 \gg 1$), even low concentrations of the impurity would render the binding profile sensitive to changes in K_1 or K_2 (i.e. $f_2 \ll 1$).

The simulations in Fig. 1 illustrate how a contaminated radioligand might be calibrated if used in parallel with a chemically pure radioligand, which could be the same or a different compound. If curve *a* represents a pure compound of known specific activity, maximal specific binding is equivalent to $[R]_t$ (i.e. $f_2 = 0$ in Eq. 6). If curve *b*, *c*, or *d* represents an impure compound, maximal specific binding equals $[R]_t/(1+f_2K_1/K_2)$. Since the true capacity is the same for the pure and impure ligands, the two estimates of B_{max} taken together yield the factor $1+f_2K_1/K_2$ for the latter compound. That, in turn, can be used as described in the Appendix to estimate the effective specific activity and hence the effective concentration of the contaminated radioligand. The factor $1+f_2K_1/K_2$ also can be calculated from the potencies of the two radioligands [i.e. $EC_{50} = K_1/(1+f_2K_1/K_2)$ in Eq. 6], but the value of K_1 must be the same or known for both compounds.

A more general approach to questions raised by an impure radioligand, and that used in the present investigation, is to formulate the model with explicit parameters for the specific activity (*SA*), the ratio f_i, and perhaps a scaling factor corresponding to the quantity $1/(1+f_2K_1/K_2)$. Data from different experimental protocols then can be pooled at will to define the system, and the values of those parameters can be optimized or fixed as required. Since all of the data contribute in the analysis, the parametric values are better defined than when estimated from B_{max} or EC_{50} alone; also, the value of *SA* or f_i can be tested for its ability to improve an otherwise unsatisfactory fit. This approach is the only practical alternative with comparatively complex models such as Scheme 1 with multiple classes of sites.

N-[^{3}H]Methylscopolamine is produced by methylation of scopolamine, which therefore is a potential contaminant in preparations of the radioligand. Mass spectra obtained for different batches of the labeled material indicate that this indeed has occurred from time to time with commercial products. In some batches, the concentration of scopolamine has been comparable to that of *N*-methylscopolamine. [^{3}H]Quinuclidinylbenzilate is produced by catalytic dehalogenation of the *p*-chloro or *p*-bromo dihalogenated precursor, and mass spectra indicate that the mono- and dihalo compounds are consistently absent from the labeled product. Commercially available [^{3}H]quinuclidinylbenzilate therefore appears to be devoid of precursor, which suggests that it can be used as a standard against which to assess the chemical purity of other muscarinic radioligands. Since any contamination is expected to reduce the values of $[R_j]_{t,app}$ and $K_{1j,app}$ (Eq. A2), the apparent capacity for [^{3}H]quinuclidinylbenzilate is expected to equal or to exceed that for *N*-[^{3}H]methylscopolamine.

A shortfall in the number of sites labeled by *N*-[^{3}H]methylscopolamine has been typical of cardiac muscarinic receptors in the present investigation. With receptors purified from porcine atria, for example, the apparent capacity

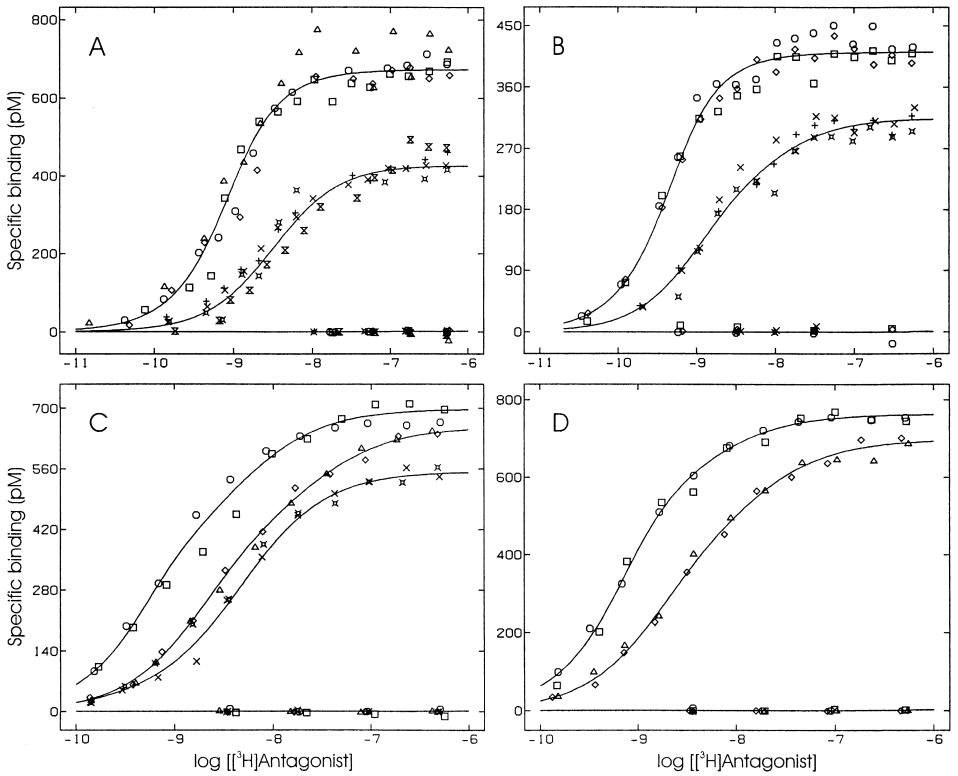

Fig. 2. Differential apparent capacity of purified m2 receptors for *N*-[^{3}H]methylscopolamine and [^{3}H]quinuclidinylbenzilate. The assays depicted in each panel were performed with the radioligand alone (upper curves) and together with 1 mM unlabeled NMS (baseline). Panels A and B: Parallel assays with [^{3}H]QNB (❍, ◇, ❑, Δ) and [^{3}H]NMS (✧, +, ×, ☒) were carried out on two different preparations of receptor, and each panel depicts the results from one preparation (A, N = 4; B, N = 3). Data from different experiments are represented by different symbols (❍, ✧; ◇, +; ❑, ×; Δ, ☒). The lot numbers for [^{3}H]QNB are as follows: A, 3329033; B, 2824273. The lot numbers for [^{3}H]NMS are: A, 3318049; B, 2924211. Panel C: Parallel assays were carried out with [^{3}H]QNB (❍, ❑, lot 3329907) and two different lots of [^{3}H]NMS (◇, Δ, lot 3406009; ✧, ×, lot 3273247) in two separate experiments, each performed on a different preparation of receptor (❍, ◇, ✧; ❑, Δ, ×). Panel D: Parallel assays were carried out with [^{3}H]QNB (❍, ❑) and [^{3}H]NMS (◇, Δ) in two separate experiments, each of which involved radioligands from a different manufacturer (NEN: ❍, [^{3}H]QNB lot 3329907; ◇, [^{3}H]NMS lot 3406009. Amersham: ❑, [^{3}H]QNB lot 44; Δ, [^{3}H]NMS lot 27); the same preparation of receptor was used throughout. The lines in each panel illustrate the best fit of Eq. 3 to all of the data represented in that panel taken together. [^{3}H]QNB and [^{3}H]NMS were designated throughout as ligands 1 and 2, respectively, and the number of classes of sites (n) was taken as 1 or 2, as required. For each radioligand, single values of K_{ij} and F_2 were common to all of the data. Single values of $[R]_t$ were common to all data from the same experiment (A–C) or from both experiments (D), irrespective of radioligand; the lower capacity for [^{3}H]NMS was accommodated by a single value of f_R common to those data. The value of $[R]_t$ thus was permitted to differ among experiments, while the relative capacity for [^{3}H]NMS and [^{3}H]QNB was assumed to be constant. The fitted values of f_R and the mean (A–C) or fitted (D) values of $[R]_t$ are as follows: A, 0.64 ± 0.02, 672 ± 53 pM (N = 4); B, 0.76 ± 0.03, 411 ± 2 pM (N = 3); C, 0.94 ± 0.03 (lot 3406009), 0.79 ± 0.02 (lot 3273247), 697 ± 94 pM (N = 2); D, 0.91 ± 0.02, 763 ± 9 pM. Other parametric values are as follows. Panel A (n = 1): log K_{11} = –9.32 ± 0.05, log K_{21} = –8.53 ± 0.03. Panel B ([^{3}H]QNB, n = 1; [^{3}H]NMS, n = 2): log K_{11} = –9.64 ± 0.03, log K_{21} = –9.03 ± 0.13, log K_{22} = –7.92 ± 0.67, $F_{2,NMS}$ = 0.23 ± 0.17. Panel C (n = 2): log K_{11} = –9.66 ± 0.17, log K_{12} = –8.29 ± 0.26, $F_{2,QNB}$ = 0.39 ± 0.12; log K_{21} = –8.77 ± 0.09, log K_{22} = –7.57 ± 0.35, $F_{2,NMS}$ = 0.30 ± 0.10 ([^{3}H]NMS lot 3406009); log K_{21} = –9.74 ± 0.70, log K_{22} = –8.33 ± 0.08, $F_{2,\ NMS}$ = 0.93 ± 0.07 ([^{3}H]NMS lot 3273247). Panel D (n = 2): log K_{11} = –9.48 ± 0.11, log K_{12} = –8.19 ± 0.42, $F_{2,QNB}$ = 0.18 ± 0.10; log K_{21} = –8.84 ± 0.09, log K_{22} = –7.80 ± 0.31, $F_{2,NMS}$ = 0.30 ± 0.12. In panels A–C, individual estimates of B_{obsd} were normalized to the mean value of $[R]_t$ for all of the curves included in the analysis, and the corresponding value of B_{sp} is plotted on the y-axis. In panel D, the values of B_{sp} were calculated from B_{obsd} taken as measured; the constraints on K_{ij}, F_2, f_R, and $[R]_t$ were without appreciable effect on the weighted sum of squares (P = 0.059).

seldom has exceeded 80% of that for [^{3}H]quinuclidinylbenzilate (e.g. Fig. 2, A and B). Binding parameters obtained with different batches of radioligand and four different preparations of receptor are summarized in Table 2. Since *N*-[^{3}H]methylscopolamine and [^{3}H]quinuclidinylbenzilate were measured in parallel in all experiments, the estimates of maximal binding are directly comparable for the two radioligands. The results suggest that most if not all of the discrepancy in capacity derives from the radioligand rather than the receptor.

The capacity for *N*-[^{3}H]methylscopolamine relative to that for [^{3}H]quinuclidinylbenzilate was only about 0.6 with one batch of *N*-[^{3}H]methylscopolamine in two successive preparations of receptor (i.e. batch 1 in preparations 1 and 2, Table 2). A somewhat higher value of about 0.8 was obtained with a second batch of *N*-[^{3}H]methylscopolamine in two additional preparations of receptor (batch 2 in preparations 3 and 4), while the same preparations yielded a value of 0.92 with two additional batches of the radioligand (batches 3 and 4 in preparations 3 and 4, respectively). The

Table 2
Empirical characterization of specific binding to purified m2 receptors

Preparation of receptor	*N*-[^{3}H]Methylscopolamine				[^{3}H]Quinuclidinylbenzilate				$\frac{B_{max,[^3H]NMS}}{B_{max,[^3H]QNB}}$
	Batch	log EC_{50}	n_H	B_{max} (pM)	Batch	log EC_{50}	n_H	B_{max} (pM)	
1 (3)	1	−7.36 ± 0.18	1.02 ± 0.18	176–366	1	−8.28 ± 0.25	0.93 ± 0.15	382–522	0.58 ± 0.07
2 (5)	1	−8.38 ± 0.18	1.00 ± 0.10	351–488	1	−9.00 ± 0.24	0.87 ± 0.10	548–829	0.63 ± 0.02
3 (6)	2	−8.29 ± 0.07	1.00 ± 0.04	442–574	2	−8.88 ± 0.06	0.94 ± 0.19	538–738	0.79 ± 0.02
3 (2)	3	−8.28 ± 0.13	0.84 ± 0.05	502–567	2	−8.97 ± 0.11	0.69 ± 0.11	538–630	0.92 ± 0.02
4 (1)	2	−8.49	0.84	628	2	−9.30	0.79	758	0.83
4 (2)	3	−8.72 ± 0.23	0.93 ± 0.11	651–729	2	−9.31 ± 0.01	0.80 ± 0.01	737–758	0.92 ± 0.04
4 (2)	4	−8.67 ± 0.02	0.89 ± 0.07	672–708	3	−9.26 ± 0.00	0.94 ± 0.08	754–767	0.91 ± 0.02

Binding was measured at graded concentrations of [^{3}H]NMS and [^{3}H]QNB as illustrated in Fig. 2. The two radioligands were used in parallel in each experiment, and the number of experiments is shown in parentheses. Data from individual experiments were analyzed in terms of Eq. 2 and Eq. 3 to obtain estimates of n_H, log EC_{50}, and B_{max} for each radioligand. When n_H was near or greater than 1, the values of EC_{50} and B_{max} were obtained from Eq. 2. When n_H was appreciably less than 1, the values of EC_{50} and B_{max} were estimated according to Eq. 3 ($n = 2$): B_{max} was taken as $[R]_t$, and EC_{50} was taken as the root of the polynomial $K_{11}K_{12} + \{K_{11}(1 - 2F_2) + K_{12}(1 - 2F_1)\}\ EC_{50} - EC_{50}^2 = 0$. The relative capacity for [^{3}H]NMS and [^{3}H]QNB was calculated for each experiment (i.e. $B_{max,[^3H]NMS}/B_{max,[^3H]QNB}$), and the individual estimates of log EC_{50}, n_H, and relative capacity were averaged to obtain the means listed in the table. Variability is indicated by the SEM ($N > 2$) or the range ($N = 2$). Lot numbers for the different batches of [^{3}H]NMS are as follows: 1, NEN lot 3318049; 2, NEN lot 3273247; 3, NEN lot 3406009; 4, Amersham lot 27. The lot numbers for [^{3}H]QNB are: 1, NEN lot 3329039; 2, lot NEN 3329907; 3, Amersham lot 44.

ratios of 0.6 and 0.8 were obtained with radiolabeled material in which the concentration of scopolamine was 85 or 75% of the concentration of *N*-[^{3}H]methylscopolamine, as determined by mass spectrometry (batches 1 and 2, respectively); ratios greater than 0.9 were found only with radiolabeled material apparently devoid of scopolamine (batches 3 and 4).

The binding of *N*-[^{3}H]methylscopolamine with and without accompanying scopolamine is compared with that of [^{3}H]quinuclidinylbenzilate in Fig. 2C, where the data were obtained in assays with all three radiolabeled products in each of two different preparations of purified receptor. As estimated empirically in terms of Scheme 1 (Eq. 3), the relative capacity for *N*-[^{3}H]methylscopolamine and [^{3}H]quinuclidinylbenzilate was 0.94 ± 0.03 in the absence of detectable scopolamine and 0.79 ± 0.02 when the concentration of scopolamine was 75% of that of *N*-[^{3}H]methylscopolamine. The same batch of [^{3}H]quinuclidinylbenzilate was used throughout, and both preparations of receptor yielded the same result with the three radioligands. The differential capacity for two different batches of *N*-[^{3}H]methylscopolamine, therefore, appears to have been caused by contaminating scopolamine.

The binding of [^{3}H]quinuclidinylbenzilate and *N*-[^{3}H]methylscopolamine from two different manufacturers is compared in Fig. 2D. Both batches of *N*-[^{3}H]methylscopolamine were devoid of scopolamine, as indicated by mass spectrometry, and the data are virtually superimposable. Two classes of sites were required for agreement with Scheme 1, and the curves represent the best fit obtained with a single set of parameters for all of the data. The sum of squares is not significantly less with a separate set of parameters for the pair of radioligands from each manufacturer ($P = 0.059$).

As described above and in the Appendix, differences in the capacity for [^{3}H]quinuclidinylbenzilate and *N*-[^{3}H]methylscopolamine can be used to estimate the effective specific activity of the latter. The lines in each panel of Fig. 2 were obtained by finding the optimal ratio of capacities for the two radioligands (i.e. f_R), and the fitted values are listed in the legend. In alternative analyses, also in terms of Eq. 3, the true value of $[R]_t$ was assumed to be the same for both radioligands (i.e. $f_R = 1$), and the value of the specific activity was optimized for *N*-[^{3}H]methylscopolamine. For each set of data, the second fit is equivalent to that shown in the corresponding panel of Fig. 2. As expected, the ratio of capacities for the two ligands equals the ratio of the optimal specific activity to the specific activity stated by the manufacturer (i.e. SA'/SA, Eq. A3 and A4. Fig. 2A, 0.63; 2B, 0.76; 2C, 0.94 and 0.79; 2D, 0.91).

The differential capacity illustrated in Fig. 2 is not unique to purified receptors. The relative capacity for *N*-[^{3}H]methylscopolamine and [^{3}H]quinuclidinylbenzilate was 0.74 ± 0.02 ($N = 5$) (Fig. 3A) and 0.76 ± 0.01 ($N = 3$) in two preparations of sarcolemmal membranes, as determined with the same lot of each radioligand. Similarly, the relative capacity was 0.69 ± 0.01 ($N = 4$) in one preparation of sarcolemmal membranes solubilized in digitonin-cholate (Fig. 3C) and 0.82 ± 0.01 in another preparation of purified receptor (Fig. 3E).

Differences in the apparent capacity for *N*-[^{3}H]methylscopolamine and [^{3}H]quinuclidinylbenzilate cannot be attributed to a subpopulation of independent sites accessible only to the latter. The inhibitory effect of unlabeled *N*-methylscopolamine on the binding of [^{3}H]quinuclidinylbenzilate to sarcolemmal membranes, to the digitonin-solubilized preparation, and to purified receptors is illustrated in Fig. 3 (right-hand panels). Assays were performed at two concentrations of the radioligand, and the number of sites labeled at the higher concentration in the absence of *N*-

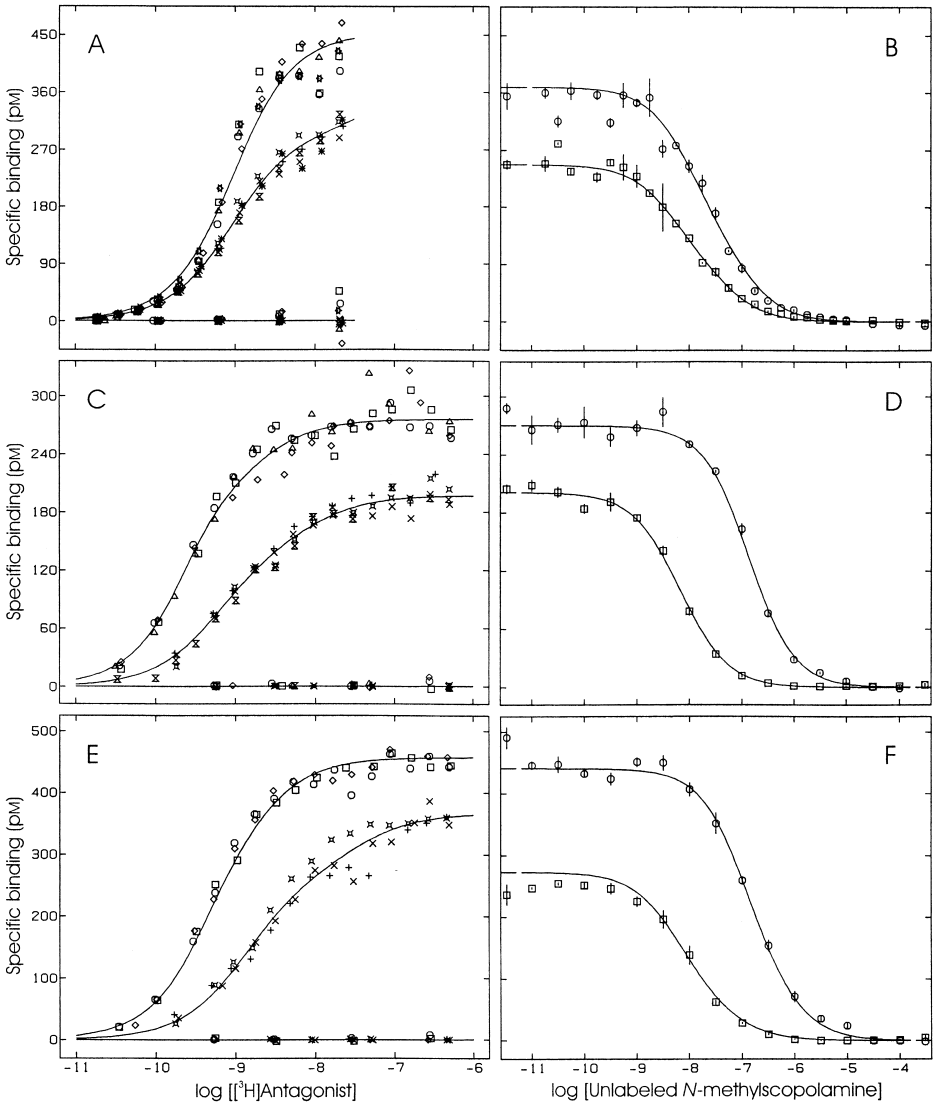

Fig. 3. Binding of quinuclidinylbenzilate and *N*-methylscopolamine to sarcolemmal membranes (A, B), to digitonin-solubilized extracts (C, D), and to purified m2 receptors (E, F). Panels A, C, and E: Parallel assays with [^{3}H]QNB (❍, ◇, ❑, Δ,☆) and [^{3}H]NMS (✧, +, ×, ⧖, ✻) were performed with the radioligand alone (upper curves) and together with 1 mM unlabeled NMS (baseline); different symbols denote data from different experiments (❍, ✧; ◇, +; ❑,×; Δ, ⧖; ☆,✻). Panels B, D, and F: Parallel assays were carried out at near-saturating (❍) and sub-saturating (❑) concentrations of [^{3}H]QNB and graded concentrations of unlabeled NMS (N = 3). The concentration of protein in the assays on sarcolemmal membranes was 0.1 g/L. For each preparation of receptor, the lines illustrate the best fit of Eq. 3 to the data represented in both panels taken together. The fitted parametric values and details of the analyses are given in Table 3. To obtain the adjusted values of B_{sp} plotted on the y-axis, the values of $[R]_t$ were taken as the mean of the individual values as follows: A and B, 454 ± 19 pM (N = 8); C and D, 276 ± 26 pM (N = 7); E and F, 457 ± 10 pM (N = 6). The mean values of log $[L_1]_t$ for the adjustment in the right-hand panels are: B, –8.97 ± 0.01 and –8.47 ± 0.01; D, –9.06 ± 0.004 and –7.66 ± 0.02; F, –9.08 ± 0.01 and –7.79 ± 0.01. Points shown at the lower and upper ends of the x-axis in panels B, D, and F indicate binding in the absence of NMS and in the presence of 1 mM NMS. The mean estimates of inhibitory potency (log IC_{50}) and the Hill coefficient (n_H) for unlabeled NMS are as follows, at the lower and higher concentrations of [^{3}H]QNB, respectively: B, –7.96 ± 0.03 and 0.81 ± 0.05, –7.58 ± 0.03 and 0.84 ± 0.02; D, –8.17 ± 0.03 and 1.07 ± 0.06, –6.86 ± 0.03 and 1.06 ± 0.03; F, –7.94 ± 0.08 and 0.98 ± 0.09, –6.81 ± 0.09 and 0.86 ± 0.01. Individual estimates of IC_{50} and n_H were obtained for each set of data according to the Hill equation [i.e., $(B_{obsd} = B_{[NMS]=0} - B_{[NMS]\to\infty})\{IC_{50}^{n_H}/([NMS]^{n_H}+IC_{50}^{n_H})\} + B_{[NMS]\to\infty}$], and the three values were averaged to obtain the means listed above.

methylscopolamine exceeded the number of sites labeled at apparently saturating concentrations of *N*-[^{3}H]methylscopolamine (left-hand panels). Moreover, the maximal binding of *N*-[^{3}H]methylscopolamine was defined by radioligand concentrations approaching 1 μM, at least in solution (Fig. 3, C and E), while the inhibition of [^{3}H]quinuclidinylbenzilate was complete or nearly so at concentrations of unlabeled *N*-methylscopolamine near 1 μM (Fig. 3, B, D, and F). The notion that some receptors are exclusive for [^{3}H]quinuclidinylbenzilate therefore implies that unlabeled *N*-methylscopolamine is inhibitory at sites inaccessible to radiolabeled *N*-methylscopolamine. While this anomaly is less apparent in membranes owing to practical limitations on the highest concentration of radioligand, the non-specific

Table 3
Affinities of [^{3}H]quinuclidinylbenzilate and *N*-[^{3}H]methylscopolamine estimated semi-empirically in terms of Scheme 1

Preparation	L	Affinity of quinuclidinylbenzilate			Affinity of *N*-methylscopolamine[a]			F_n^b
		log K_{11}	log K_{12}	log K_{13}	log K_{21}	log K_{22}	log K_{23}	
Sarcolemmal membranes	^{3}H (5)	−9.15 ± 0.11	−9.16 ± 0.20	[c]	−9.11 ± 0.03	−6.72 ± 0.48[d]		} 0.33 ± 0.03
	^{1}H (3)				−8.69 ± 0.08	−7.77 ± 0.24	[c]	
Solubilized in digitonin-cholate	^{3}H (4)	−10.09 ± 0.05[e]	−10.09 ± 0.05[e]	−8.83 ± 0.08	−9.28 ± 0.08	−8.13 ± 0.34	>−5.7	} 0.29 ± 0.01
	^{1}H (3)				−9.27 ± 0.09[f]	−9.27 ± 0.09[f]	−8.18 ± 0.26	
Purified in digitonin-cholate	^{3}H (3)	−9.85 ± 0.07	−8.96 ± 0.37	−8.83 ± 0.31	−8.93 ± 0.06	−7.53 ± 0.32	>−6.4	} 0.20 ± 0.02
	^{1}H (3)				−9.02 ± 0.13	−8.07 ± 0.57	−7.28 ± 0.36	

Data illustrated in the paired left- and right-hand panels of Fig. 3 were analyzed according to Eq. 3 ($n = 2$ or 3) to obtain the fitted curves shown in the figures and the parametric values listed in the table. QNB was present only as the radioligand (L = ^{3}H, both panels of Fig. 3), while NMS was present as either the radioligand (L = ^{3}H, left-hand panels) or the unlabeled analogue (L = ^{1}H, right-hand panels). The number of experiments is shown in parentheses. For QNB, a single value of each K_{1j} was common to all of the data shown in the right-hand panel and to those data acquired at graded concentrations of [^{3}H]QNB in the left-hand panel. For NMS, a single value of each K_{2j} was common to all of the data shown in the right-hand panel, and a second value was common to those data acquired at graded concentrations of [^{3}H]NMS in the left-hand panel. A difference between the two fitted values of K_{2j} constitutes a discrepancy between the model and the data. Single values of F_j were common to all of the data shown in both panels. Single values of $[R]_t$ were common to all data acquired within the same experiment, and single values of *NS* were common to data acquired with the same radioligand in the same experiment. The lot numbers for [^{3}H]QNB and [^{3}H]NMS are as follows: membranes, 3186289 and 3144205; solubilized preparation, 3231205 and 3144205; purified receptor, 3186289 and 3144205.

[a] [^{3}H]NMS and [^{3}H]QNB shared a single value of $[R]_t$ when both radioligands were measured in parallel, and the lower capacity for [^{3}H]NMS is accounted for by anomalously weak binding at some of the sites. The corresponding values of K_{2j} for [^{3}H]NMS are undefined for solubilized and purified material ($j = 3$), and the parameter therefore was mapped to obtain the lower bound as identified by a significant increase in the weighted sum of squares ($P < 0.05$). At higher values of K_{23}, the parameter is without effect on the sum of squares or on the values of other parameters; the latter were evaluated with the value of K_{23} set at 0.1 M.

[b] F_n represents the fraction of sites exhibiting lowest affinity for [^{3}H]NMS and corresponds to either F_2 or F_3. The values of F_2 when n is 3 are as follows: solubilized preparation, 0.19 ± 0.07; purified receptor, 0.21 ± 0.05. The quantity $1 - F_n$ approximates the relative capacity of the preparation for [^{3}H]NMS and [^{3}H]QNB.

[c] Two classes of sites are sufficient for the model to describe the data.

[d] The value exceeds the highest concentration of the radioligand but is defined by a shallow minimum in the weighted sum of squares.

[e,f] The two parameters are indistinguishable and therefore were optimized as a single value.

binding of [^{3}H]quinuclidinylbenzilate was the same in the presence of either 0.01 mM unlabeled quinuclidinylbenzilate or 0.1 mM *N*-methylscopolamine.

Receptors that bind [^{3}H]quinuclidinylbenzilate but not *N*-[^{3}H]methylscopolamine constitute an example of Scheme 1, which can be examined quantitatively by fitting Eq. 3 to the combined data illustrated in the left- and right-hand panels of Fig. 3. The lines represent the fitted curves, and the corresponding parametric values are listed in Table 3. Quinuclidinylbenzilate and *N*-methylscopolamine were designated as ligands 1 and 2, and the corresponding affinities are therefore K_{1j} and K_{2j}. Each analysis was arranged such that all of the data shared common values of F_j, in accord with the presumption that there is no interconversion among the different states or forms of the receptor. Similarly, the affinity of quinuclidinylbenzilate for each state was estimated as the single value of K_{1j} common to all data acquired with [^{3}H]quinuclidinylbenzilate as the radioligand. In contrast, the affinity of *N*-methylscopolamine for each state was estimated as two parameters: one value of K_{2j} derived from the binding of *N*-[^{3}H]methylscopolamine alone (left-hand panel), and a second value derived from the inhibitory effect on [^{3}H]quinuclidinylbenzilate (right-hand panel). Since the labeled and unlabeled analogues of *N*-methylscopolamine are expected to be functionally identical, any appreciable difference in the two values of K_{2j} constitutes a discrepancy between the model and the data. In that event, the analysis is essentially empirical despite the mechanistic basis of Eq. 3.

Owing to the difference in apparent capacity, at least two classes of sites are required to describe the system under all conditions: one class that binds both radioligands, and a second that exhibits anomalously low affinity for *N*-[^{3}H]methylscopolamine. Three classes of sites are required for solubilized and purified receptors in order to accommodate a small degree of dispersion in the binding of both radioligands ($n_H = 0.76$ to 0.89). In each case, the affinity of *N*-[^{3}H]methylscopolamine for the sites labeled only by [^{3}H]quinuclidinylbenzilate is poorly defined by the data. When three classes of sites are required, the value of K_{23} is defined only by a lower bound estimated by mapping. The values of F_2 or F_3 listed in the table indicate the fraction of sites inaccessible to *N*-[^{3}H]methylscopolamine at the concentrations used in the assays.

The affinities listed for *N*-methylscopolamine in Table 3 highlight the discrepancy between its binding as measured directly and as inferred from its inhibitory effect on the binding of [^{3}H]quinuclidinylbenzilate. In all preparations, the lower capacity for *N*-[^{3}H]methylscopolamine implies an equilibrium dissociation constant that exceeds the highest concentration of radioligand used in the assays; thus, the highest affinity commensurate with those data differs by

Table 4
Assessment of Scheme 1 for binding to purified m2 receptors

Classes of sites (n)	NMS: two values of K_{2j}		NMS: one value of K_{2j}	
	WSSQ	P	WSSQ	P
1	42,470 (195)		42,940 (196)	
2	13,960 (191)	<0.00001	25,780 (193)	<0.00001
3	13,220 (187)	0.037	25,200 (190)	0.23
4	12,840 (183)	0.25	25,200 (187)	

Data illustrated in panels E and F of Fig. 3 were analyzed according to Eq. 3 (n = 1–4), and the weighted sum of squares (WSSQ) from each analysis is listed in the table. The number of degrees of freedom is shown in parentheses. The radiolabeled and unlabeled analogues of NMS were assumed to have different affinities (i.e. two values of K_{2j}) or the same affinity (i.e. one value of K_{2j}) for each class of sites, and parameters otherwise were assigned as described in the footnotes to Table 3. Within each series of analyses, the values of P were calculated from the F-statistic for the decrease in the sum of squares associated with each additional class of sites. The fitted curves obtained with two values of K_{2j} when n is taken as 3 are illustrated in Fig. 3, and the corresponding parametric values are listed in Table 3.

10-fold or more from the weakest affinity inferred from the inhibition of [^{3}H]quinuclidinylbenzilate. To confirm these anomalies, the analyses summarized in Table 3 were repeated with the parameters assigned strictly in accord with the model: that is, the affinity of *N*-methylscopolamine at each class of sites was assumed to be the same for binding of the radioligand alone and for the inhibition of [^{3}H]quinuclidinylbenzilate. This constraint is accompanied in each case by a substantial increase in the sum of squares ($P < 0.00001$), and the fitted curves show marked deviations from the data.

Inconsistencies in the affinity of *N*-methylscopolamine cannot be reconciled by increasing the degree of heterogeneity, as illustrated for purified receptors by the results summarized in Table 4. With different affinities for radiolabeled and unlabeled *N*-methylscopolamine at each class of sites, the weighted sum of squares is found to decrease from 42,470 when n is 1 to about 13,000 when n is 3 or more; with a single affinity, the sum of squares is 42,940 when n is 1 and decreases to 25,200 when n is 3 or more (Table 4). Thus, the asymptotic sum of squares at any value of n greater than 4 is doubled when the parameters are assigned in a mechanistically consistent manner. It follows that the data are inconsistent with Scheme 1 regardless of the number of classes of sites, and the model can be rejected categorically. Similar results are obtained for the other preparations represented in Table 3.

The failure of Scheme 1 suggests that the inhibitory effect of unlabeled *N*-methylscopolamine on the binding of [^{3}H]quinuclidinylbenzilate is at least partly non-competitive or that the estimated capacity for *N*-[^{3}H]methylscopolamine is artifactually low. The presence of scopolamine in several batches of *N*-[^{3}H]methylscopolamine points to an artifact, and the anomalies that emerge from Scheme 1 are avoided if the unlabeled ligand is included in the analysis. The data illustrated in Fig. 4A are representative of six experiments in which the relative apparent capacity for *N*-[^{3}H]methylscopolamine and [^{3}H]quinuclidinylbenzilate was 0.79 ± 0.02. The same batch of each radioligand was used throughout. The data illustrated in Fig. 4B are from three experiments in which scopolamine and unlabeled *N*-methylscopolamine were characterized for their inhibitory effects at two concentrations of [^{3}H]quinuclidinylbenzilate. The pooled data define all of the parameters of Scheme 1, including the concentration of scopolamine relative to that of *N*-[^{3}H]methylscopolamine in assays at graded concentrations of the latter (i.e. f_3 in Eq. 4 when scopolamine is designated as ligand 3). Such provision for contaminating scopolamine avoids the discrepancy that otherwise occurs between labeled and unlabeled *N*-methylscopolamine, and the model can account for the data in both panels of Fig. 4 taken together. The fitted value of f_3 for the amount of scopolamine in the assays with *N*-[^{3}H]methylscopolamine is 2.3 ± 0.4; the corresponding value estimated from electrospray mass spectrometry of a sample from the same batch of the radioligand is 0.75.

Binding profiles obtained with two batches of *N*-[^{3}H]methylscopolamine and aliquots from the same batch of purified receptor are illustrated in Fig. 5. One batch of the radioligand was devoid of scopolamine (i.e. $f_3 = 0$) (Fig. 5A), as indicated by mass spectra recorded by the manufacturer and locally, and one contained scopolamine and *N*-[^{3}H]methylscopolamine in similar amounts (i.e. $f_3 = 0.75$) (Fig. 5B). The latter batch was the same as that used to obtain the data illustrated in Fig. 4A. In each case, binding was measured with the radioligand taken as supplied by the manufacturer (curve *a*) and supplemented with scopolamine at three different molar ratios over a 10-fold range from 2 to about 20 (curves *b–d*). The conditions of the experiments represented in panels A and B of Fig. 5 thus mimic the assumptions underlying the simulations in Fig. 1. Also shown are data on the binding of [^{3}H]quinuclidinylbenzilate at graded concentrations of either scopolamine or unlabeled *N*-methylscopolamine (Fig. 5D) and at graded concentrations of the radioligand (Fig. 5C). All of the parameters of Scheme 1 are defined by the data represented in panels A–D taken together. The lines represent the best fit obtained from a mechanistically consistent analysis of the pooled data, and the fitted parametric values are listed in the legend to the figure.

The results shown in Fig. 5 illustrate the effect of an unrecognized contaminant on the binding profile of a radioligand, and they provide further evidence that scopolamine is responsible for discrepancies between the data and Scheme 1. Based on the affinity of scopolamine defined by the data in panels C and D of Fig. 5 (i.e. K_{3j}) and on the total concentration determined as described below, the model can account for the difference in the apparent capacity of purified receptors for two different batches of the radioligand (cf. panels A and B of Fig. 5) and for the changes that occur when the radiolabeled material is supplemented with scopolamine. To obtain the fit shown in Fig. 5, the total con-

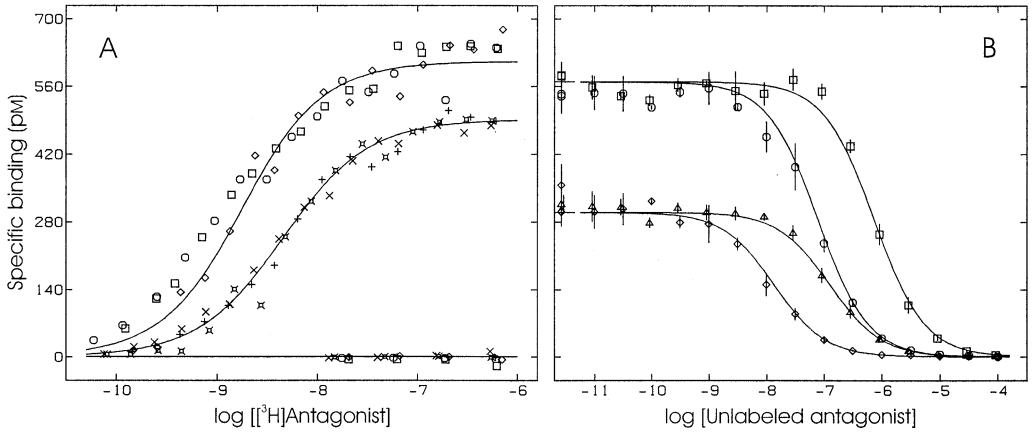

Fig. 4. Contribution of scopolamine to discrepancies between Scheme 1 and the binding of [^{3}H]quinuclidinylbenzilate and *N*-[^{3}H]methylscopolamine to purified m2 receptors. Panel A: Parallel assays with [^{3}H]QNB (❍, ◇, ❑) and [^{3}H]NMS (✧, +, ×) were performed with the radioligand alone (upper curves) and together with 1 mM unlabeled NMS (baseline); different symbols denote data from different experiments (N = 3). Panel B: Parallel assays were performed at near-saturating (❍, ❑) and sub-saturating (◇, Δ) concentrations of [^{3}H]QNB and graded concentrations of both unlabeled NMS (❍, ◇) and scopolamine (❑, Δ); thus, each experiment comprised four sets of data (N = 3). [^{3}H]QNB and [^{3}H]NMS were from lots 3329907 and 3273247, respectively. The lines illustrate the best fit of Eq. 3 ($n = 1$) to the data represented in both panels taken together. QNB, NMS, and scopolamine were designated as ligands 1, 2, and 3, respectively. The concentration of scopolamine in panel A was defined relative to that of [^{3}H]NMS (i.e. $f_3 = [L_3]_t/[L_2]_t$). Single values of K_{2j} and K_{3j} were common to all of the data. Values of K_{1j} were assigned separately to the data represented in each panel in order to accommodate a small difference in the affinity of [^{3}H]QNB as defined by graded concentrations of the radioligand (A) and that inferred from the effect of [^{3}H]QNB on the inhibitory behavior of unlabeled NMS and scopolamine (B). Single values of $[R]_t$ were common to all data from the same experiment, irrespective of radioligand, and a single value of f_3 was common to all of the data obtained at graded concentrations of [^{3}H]NMS. The fitted value of f_3 is 2.3 ± 0.4, and the estimates of affinity are as follows: log K_{11} = –9.10 ± 0.02 (A, QNB), log K_{11} = –8.84 ± 0.03 (B, QNB), log K_{21} = –8.28 ± 0.02 (NMS), and log K_{31} = –7.30 ± 0.03 (scopolamine). Individual estimates of B_{obsd} were normalized to the mean value of $[R]_t$ for all of the data included in the analysis (i.e. $[R]_t$ = 611 ± 18 pM, N = 6), and the corresponding value of B_{sp} is plotted on the y-axis. The mean values of log $[L_1]_t$ for the adjustment in panel B are –7.94 ± 0.01 and –8.97 ± 0.02. Points shown at the lower end of the x-axis in panel B indicate binding at concentrations of unlabeled antagonist below 10 pM.

centration of scopolamine was taken as the sum of that added in the experiment plus that present with *N*-[^{3}H]methylscopolamine as received from the manufacturer; the former was entered explicitly for each value of B_{obsd}, and the latter was calculated from the concentration of *N*-[^{3}H]methylscopolamine and the appropriate value of f_3. In the case of Fig. 5A, the radiolabeled product was apparently devoid of scopolamine, and the value of f_3 was taken as zero. In the case of Fig. 5B, the amount of contaminating scopolamine is given by the single value of f_3 common to all of the data, and the fitted estimate is 1.4 ± 0.2.

Both values of f_3 estimated from the binding properties (i.e. 2.3 ± 0.4, Fig. 4; 1.4 ± 0.2, Fig. 5) exceed the value estimated by mass spectrometry (0.75). The value of 2.3 is a measure of the differential capacity for *N*-[^{3}H]methylscopolamine and [^{3}H]quinuclidinylbenzilate (Fig. 4A). Part of that difference can be attributed to the comparatively rapid dissociation of *N*-[^{3}H]methylscopolamine from the receptor, which can lead to a loss of 3–7% of the bound radioligand on the columns of Sephadex G-50 used in the binding assays. No corresponding loss occurs with [^{3}H]quinuclidinylbenzilate, which undergoes no appreciable dissociation under the same conditions. The difference in the rate of dissociation also accounts, in all likelihood, for the small difference in capacity between [^{3}H]quinuclidinylbenzilate and *N*-[^{3}H]methylscopolamine devoid of scopolamine (Fig. 2C). To correct for loss through dissociation, the data represented in Fig. 4 were refitted with the value of $[R]_t$ for *N*-[^{3}H]methylscopolamine adjusted downward by the factor f_R. The value of f_3 decreases with f_R, as shown in Fig. 6, and equals 1.4 when f_R is set at 0.92. The same value of f_3 was obtained from the analysis illustrated in Fig. 5, where *N*-[^{3}H]methylscopolamine is compared with uncontaminated *N*-[^{3}H]methylscopolamine rather than with [^{3}H]quinuclidinylbenzilate as in Fig. 4. When the comparison is between two batches of the same radioligand, the value of f_3 is independent of f_R.

The foregoing considerations indicate that different approaches yield consistent results when the value of f_3 is inferred from binding assays. The remaining discrepancy between the value of 1.4 and the value estimated by mass spectrometry appears to arise primarily from the underrepresentation of scopolamine in the mass spectrum. The results summarized in Table 5 were obtained with samples prepared at molar ratios of scopolamine to *N*-methylscopolamine between 0.20 and 2.3. The corresponding ratio based on the size of the two peaks was consistently less, and a value of 0.75 was obtained when scopolamine and *N*-methylscopolamine were injected in equimolar amounts. The discrepancy suggests that scopolamine ionizes less efficiently than does the methylated product, and it can account for most if not all of the difference in f_3 between the value of 1.4 inferred from the binding assays and that of 0.75 revealed in the mass spectrum. Scopolamine was absent from the spectrum when *N*-methylscopolamine was injected alone and therefore does not occur as a fragmentation product.

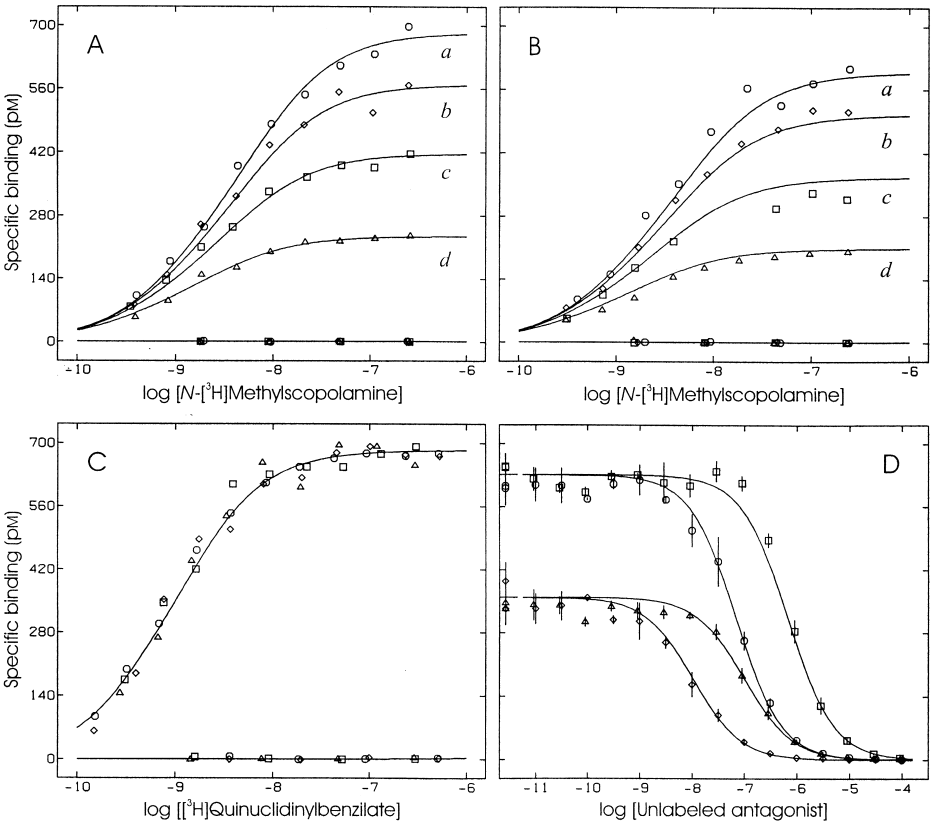

Fig. 5. Effect of scopolamine on the binding of *N*-[^{3}H]methylscopolamine to purified m2 receptors. Panels A and B: Two lots of [^{3}H]NMS (A, lot 3406009; B, lot 3273247) were compared for binding in the presence of scopolamine, which was premixed with the radioligand prior to preparing the graded dilutions used in the assays. Aliquots from the same batch of purified receptor were used throughout. In each case, parallel assays were performed with the radioligand alone (❍, curve *a*), the radioligand plus added scopolamine (◇, ❑, Δ; curves *b*–*d*), and the radioligand plus 1 mM unlabeled NMS (baseline). The molar ratios of scopolamine to *N*-[^{3}H]methylscopolamine in panels A and B, respectively, are as follows: ◇, 1.96 and 2.06; ❑, 6.23 and 7.02; Δ, 18.7 and 20.8. Panel C: Binding of [^{3}H]QNB was measured with the radioligand alone (upper curve) and together with 1 mM unlabeled NMS (baseline); different symbols denote data from different experiments (N = 4), which included radioligand from two manufacturers (❍, ❑, NEN lot 3329907; ◇, Δ, Amersham lot 44). Panel D: Parallel assays were performed at two concentrations of [^{3}H]QNB and graded concentrations of both unlabeled NMS (❍, ◇) and scopolamine (❑, Δ), as described in the legend to Fig. 4. The same data are shown in Figs. 4B and 5D. The lines illustrate the best fit of Eq. 3 ($n = 2$, $P < 0.00001$) to the data represented in all panels taken together. QNB, NMS, and scopolamine were designated as ligands 1, 2, and 3, respectively. The concentration of scopolamine present as a contaminant in panels A and B was defined relative to the concentration of [^{3}H]NMS (i.e. $f_3 = [L_3]_t/[L_2]_t$). Single values of K_{ij} and F_2 were common to all of the data. A single value of $[R]_t$ was common to all of the data represented in panels A and B; single values of $[R]_t$ were common to the data for each pair of curves in panel C (i.e. ± unlabeled NMS) and to the data from each experiment in panel D. The value of f_3 was taken as zero for the data in panel A, and the fitted value of f_3 common to all of the data in panel B is 1.39 ± 0.22. The fitted estimates of K_{ij} are as follows: $\log K_{11} = -10.03 \pm 0.14$, $\log K_{12} = -8.87 \pm 0.09$, $\log K_{21} = -9.18 \pm 0.12$, $\log K_{22} = -8.17 \pm 0.08$, $\log K_{31} = -8.17 \pm 0.16$, $\log K_{32} = -7.19 \pm 0.08$, $F_2 = 0.67 \pm 0.07$. Individual estimates of B_{obsd} were normalized to the mean value of $[R]_t$ for all of the data included in the analysis ($[R]_t = 684 \pm 33$ pM, N = 8), and the corresponding value of B_{sp} is plotted on the y-axis. The mean values of $\log [L_1]_t$ for the adjustment in panel D are –7.94 ± 0.01 and –8.97 ± 0.02.

4. Discussion

Various preparations from porcine atria have revealed a marked difference in the apparent capacity of muscarinic receptors for the antagonists *N*-[^{3}H]methylscopolamine and [^{3}H]quinuclidinylbenzilate. Such differences have been noted previously, and they typically are attributed to heterogeneity among the receptors *per se* or to their differential localization within the preparation. Neither explanation seems plausible for the present data, which are inconsistent with the underlying premise of distinct, non-interconverting, and mutually independent sites; rather, the discrepancy in capacity can be attributed to an artifact involving *N*-methylscopolamine and its unreacted precursor scopolamine.

Three lots of *N*-[^{3}H]methylscopolamine used in the present investigation were found to contain scopolamine at concentrations comparable to those of the radioligand (i.e. $f_i = 0.75$–1.2 in Eq. 4). The capacity for [^{3}H]quinuclidinylbenzilate consistently exceeded that for *N*-[^{3}H]methylscopolamine from those lots and from other lots for which the mass spectrum is unavailable. Only when scopolamine was absent from the mass spectrum did the capacity for *N*-[^{3}H]methylscopolamine approximate that for [^{3}H]quinuclidinylbenzilate (i.e. $f_R > 0.9$ in Eq. 3), which appears to be consistently devoid of such impurities. Different batches of receptor behaved

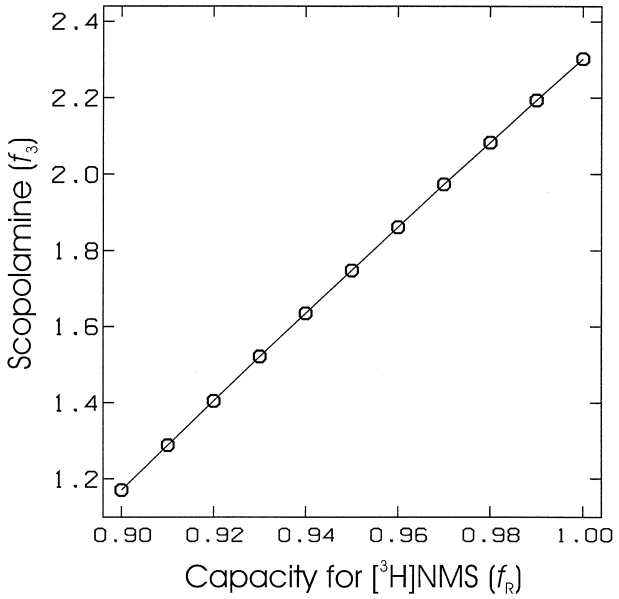

Fig. 6. Contribution of scopolamine and the loss of bound *N*-[^{3}H]methylscopolamine to the differential capacity for *N*-[^{3}H]methylscopolamine and [^{3}H]quinuclidinylbenzilate. The data represented in both panels of Fig. 4 were analyzed in terms of Eq. 3 with f_R for [^{3}H]NMS fixed at different values between 0.9 and 1.0. The fitted values of f_3, representing the molar ratio of contaminating scopolamine to [^{3}H]NMS (i.e. $[L_3]_t/[L_2]_t$), are plotted on the y-axis. Further details of the analysis are described in the legend to Fig. 4.

similarly with the same lot of *N*-[^{3}H]methylscopolamine, and different lots of *N*-[^{3}H]methylscopolamine behaved differently with the same batch of receptor.

If the scopolamine is disregarded, analyses based on Scheme 1 lead to a discrepancy between the differential capacity for the two radioligands and the inhibitory effect of *N*-methylscopolamine on the binding of [^{3}H]quinuclidinylbenzilate: labeled and unlabeled *N*-methylscopolamine differ in their apparent affinity, and the ligand therefore appears to inhibit at sites to which it does not bind. When scopolamine is included as an explicit variable, the paradox is resolved, and Scheme 1 can account simultaneously for the binding of *N*-[^{3}H]methylscopolamine and its unlabeled analogue (i.e. Fig. 4). Similarly, the model is in good agreement with the pattern of decreasing capacity that emerges when binding is measured at graded concentrations of scopolamine and *N*-[^{3}H]methylscopolamine—both pure and impure—taken together over a 10-fold range of constant molar ratio (Fig. 5).

The analyses also can be used to estimate the amount of scopolamine present with the radioligand, and those estimates can be compared with the values obtained by mass spectrometry. Thus, the value of f_i for scopolamine in one batch of *N*-[^{3}H]methylscopolamine was 2.3 as determined from the difference in the apparent capacity for *N*-[^{3}H]methylscopolamine and [^{3}H]quinuclidinylbenzilate (Fig. 4). A somewhat lower value of 1.4 was obtained when the same batch of contaminated *N*-[^{3}H]methylscopolamine and a scopolamine-free batch were supplemented with additional scopolamine (Fig. 5). The difference can be attributed to the loss of some *N*-[^{3}H]methylscopolamine when the labeled receptor is desalted on Sephadex G-50, and the higher value of f_i is therefore an overestimate. The value of 1.4 obtained from pharmacological assays exceeds that of 0.75 calculated from the mass spectrum, but the mass spectrum appears to underestimate the amount of scopolamine relative to its *N*-methylated derivative.

The situation that arises in the case of scopolamine and *N*-[^{3}H]methylscopolamine is comparatively benign. Since the dissociation constant of the impurity (L_2) is about 10-fold higher than that of the radiolabeled probe (L_1) (i.e. $K_1/K_2 = 0.1$ in Eq. 6), small amounts of the former are expected to be without appreciable effect on the binding profile of the latter. If f_2 were 0.1, for example, maximal binding would represent 99% of the true capacity (i.e. $1+f_2K_1/K_2 = 1.01$ in Eq. 6). In the present investigation, however, much higher levels of scopolamine were present in some batches of *N*-[^{3}H]methylscopolamine. The countervailing effect of f_2 on an otherwise favorable value of K_1/K_2, therefore, was sufficient to effect an appreciable reduction in the apparent capacity for the radioligand.

When the value of K_1/K_2 approximates or exceeds 1, substantial effects will occur at concentrations of an impurity that are comparatively low and perhaps difficult to avoid. One such example appears to be *N*-[^{3}H]methylquinuclidinylbenzilate, which is obtained by methylation of the precursor quinuclidinylbenzilate. With purified receptors from porcine atria, the apparent capacity for *N*-[^{3}H]methylquinuclidinylbenzilate was reported to be only about 12% of that for [^{3}H]quinuclidinylbenzilate [15]. Values between 2 and 100% have been obtained subsequently.[3] Mass spectra provided by the manufacturer indicate that the ratio of unlabeled quinuclidinylbenzilate to *N*-[^{3}H]methylquinuclidinylbenzilate has varied from 0.02 to 1.6 in different batches of the latter; moreover, experiments analogous to those represented in Fig. 4B have shown that the dissociation constant of quinuclidinylbenzilate is about 10-fold lower than that of *N*-methylquinuclidinylbenzilate.[3] *N*-[^{3}H]Methylscopolamine and *N*-[^{3}H]methylquinuclidinylbenzilate, therefore, represent two contrasting situations in which the relative affinity of the radioligand and the unlabeled precursor is favorable on the one hand (i.e. $K_1/K_2 = 0.1$) and unfavorable on the other (i.e. $K_1/K_2 = 10$). The purity of the radioligand is particularly important in the case of *N*-[^{3}H]methylquinuclidinylbenzilate.

It has been noted previously that the maximal binding of [^{3}H]quinuclidinylbenzilate can exceed that of *N*-[^{3}H]methylscopolamine and other radiolabeled antagonists in suspensions of intact cells from chick heart [16,17] and in myo-

[3] Sum CS and Wells JW, unpublished observations.

Table 5
Detection of scopolamine and *N*-methylscopolamine by mass spectrometry

Mode	Scopolamine:*N*-methylscopolamine			Relative efficiency of scopolamine	
	Molar ratio (*A*)	Peak area (*B*)	Peak height (*C*)	Peak area (*B*/*A*)	Peak height (*C*/*A*)
Selective ion monitoring	0.20	0.13 ± 0.01	0.13 ± 0.01	0.66	0.63
	0.40	0.25 ± 0.04	0.28 ± 0.05	0.63	0.70
	0.60	0.45 ± 0.01	0.51 ± 0.02	0.75	0.84
	0.80	0.62 ± 0.01	0.63 ± 0.01	0.77	0.78
	1.00	0.73 ± 0.05	0.75 ± 0.06	0.73	0.75
Full scan	0.43	0.30 ± 0.05	0.31 ± 0.05	0.69	0.73
	1.0	0.68 ± 0.06	0.72 ± 0.06	0.68	0.72
	2.3	1.3 ± 0.1	1.2 ± 0.1	0.57	0.52

Scopolamine and NMS were dissolved in ethanol at a total concentration of 100 μM and the molar ratios shown in the table. The two peaks were monitored either selectively or by full spectral scan, and the size was determined by area and by height. The amount of scopolamine is shown relative to the amount of NMS, and that ratio is shown relative to the molar ratio in the sample. Each mixture was sampled twice, and the means of the two determinations are listed in the table. The molar ratio corresponds to the parameter f_i in Eq. 4 when the radioligand is [^{3}H]NMS.

cardial homogenates [10,18–20]. Similar differences have been found with intact 1321N1 astrocytoma cells [21] and with membranes from 1321N1 cells [22], NG108–15 neuroblastoma × glioma cells [22], and rat brain [19,23–25]. Although widespread, such apparent discrepancies are not universal. The maximal binding of *N*-[^{3}H]methylscopolamine and [^{3}H]quinuclidinylbenzilate was found to be the same with intact CHO and heart cells [26,27] and with membranes from rat cortex [28]. With intact SK-N-SH neuroblastoma cells, there was a difference in capacity at 0° but not at 37° [29]. With 1321N1 cells, the capacity of intact cells for *N*-[^{3}H]methylscopolamine was 70–100% of the capacity of membranes for [^{3}H]quinuclidinylbenzilate [30]. In one study of 1321N1 cells and NG108–15 hybrids, a difference was found with membranes but not with the parent cells [22].

Owing to the lipophilic nature of quinuclidinylbenzilate, differences in the apparent capacity for *N*-[^{3}H]methylscopolamine and [^{3}H]quinuclidinylbenzilate often have been attributed to a subset of receptors that are sequestered in a compartment inaccessible to *N*-methylscopolamine. Also, it has been suggested that *N*-methylscopolamine may recognize pharmacologically distinct subtypes of the receptor [25]. As shown with probes such as [^{3}H]AF-DX 384, subtype-specific antagonists can label selectively in preparations known or expected to contain a mixture of isoforms [31,32]. Finally, kinetic evidence for isomerization of the ligand–receptor complex has led to the suggestion that some receptors may be in a state of low affinity for charged ligands [17]. Such effects may contribute to the differential capacity found in some instances, but they cannot account for the present data and seem unlikely to be wholly responsible for earlier results.

There are five known isoforms of muscarinic receptor [33,34]. When studied individually in membranes from CHO-K1 and *Sf*9 cells, they differ by less than 10-fold in their affinity for *N*-[^{3}H]methylscopolamine [35–38]; moreover, the Hill coefficient of *N*-[^{3}H]methylscopolamine typically is indistinguishable from 1 when the population of labeled sites is known to be heterogeneous and appears as such to subtype-specific ligands (e.g. Refs. 28 and 39). *N*-Methylscopolamine, therefore, shows little selectivity among muscarinic subtypes, at least in membranes. Some preferences emerge when receptor-containing *Sf*9 membranes are solubilized in digitonin-cholate, including a 90-fold difference between m2 and m3 receptors [37]. Nonetheless, known differences in affinity are insufficient to account for the shortfalls in capacity described here or, by and large, for those reported previously. Also, receptors for the present investigation were obtained from porcine atria, and cardiac muscarinic receptors generally are thought to be wholly or predominantly m2 [40]. Recent studies have suggested that the complement of subtypes is species-dependent (e.g. Refs. 41 and 42), and rat heart has been shown to contain both m1 and m2 subtypes [43], but muscarinic receptors in porcine heart appear to be exclusively m2 [44,45].

In studies on desensitization and trafficking, the maximal binding of *N*-[^{3}H]methylscopolamine to whole cells is widely used to estimate the number of receptors at the extracellular surface and thereby to follow agonist-induced sequestration (e.g. Refs. 46–57). The maximal binding of [^{3}H]quinuclidinylbenzilate is often used to control for changes in the total number of receptors (e.g. Refs. 46–55). Although the two radioligands are not always compared directly, the capacity for *N*-[^{3}H]methylscopolamine has been 50–60% of that for [^{3}H]quinuclidinylbenzilate in untreated HEK293 cells [50,54] and 80–90% or more in untreated CHO cells [51,52,55]. The possible presence of scopolamine suggests that the capacity for *N*-[^{3}H]methylscopolamine may have been underestimated in absolute terms, but changes attributed to sequestration typically are expressed relative to the binding of *N*-[^{3}H]methylscopolamine in an untreated control. Provided that the same batch of radioligand was used throughout the experiment, an artifactual change in capacity would require that the treatment

affect the ratio of affinities for *N*-[^{3}H]methylscopolamine and scopolamine (e.g. K_1/K_2 in Eq. 6). Moreover, the internalization inferred from changes in the capacity for *N*-[^{3}H]methylscopolamine has been confirmed by a loss of receptors from the plasma membrane, as revealed on sucrose density gradients [30,52] and by confocal microscopy [51,52,54–56].

The restricted access that can occur with intact cells is not expected in solution, nor can it explain the differences described here for membranes or for solubilized preparations. Sequestration and subcellular localization represent specific examples of Scheme 1, as do other potential sources of heterogeneity such as differences in post-translational processing. In each case, a differential capacity requires that the receptor cannot migrate from one compartment to another or interconvert from one form to another under the conditions of the binding assays (e.g. see Eq. 62 in Ref. 11). All such possibilities can be ruled out by the inhibitory effect of unlabeled *N*-methylscopolamine on the binding of [^{3}H]quinuclidinylbenzilate at near-saturating concentrations of the latter. Sequestration represents a special case in that the intrinsic affinity of the receptor is unchanged, and the exclusion of *N*-[^{3}H]methylscopolamine from the relevant compartment therefore must be absolute. In the likely event of leakage, the lower capacity is a kinetic effect arising from restricted diffusion and failure to attain equilibrium. In the present investigation, however, a 2.4-fold increase in the time of incubation was without effect on the binding profile obtained for either radioligand with sarcolemmal membranes or with purified receptors.

In the present investigation, the inhibition of [^{3}H]quinuclidinylbenzilate by unlabeled *N*-methylscopolamine has been characterized by Hill coefficients near 1 (e.g. $n_H > 0.8$, Fig. 3). This leads to the discrepancy with Scheme 1 when scopolamine is disregarded, since the inferred affinity of unlabeled *N*-methylscopolamine for all sites is comparable to that of *N*-[^{3}H]methylscopolamine for the labeled subset (Table 3). These results differ from the pattern described in some earlier reports on the differential capacity for *N*-[^{3}H]methylscopolamine and [^{3}H]quinuclidinylbenzilate. With muscarinic receptors in homogenates from rat brain [23,25] and in whole cells from chick heart [17], the inhibitory effect of unlabeled *N*-methylscopolamine on the binding of [^{3}H]quinuclidinylbenzilate extended over a broad range of concentration (n_H = 0.4 to 0.6) and appeared distinctly biphasic. In terms of Scheme 1 (n = 2), the affinity of unlabeled *N*-methylscopolamine for the sites of each class differed by 310- to 450-fold. The higher affinity was comparable in magnitude to that defined by graded concentrations of *N*-[^{3}H]methylscopolamine, while the lower affinity was sufficiently weak for those sites to be unobservable in the binding of the radioligand.

On the basis of affinities alone, the biphasic profile traced by unlabeled *N*-methylscopolamine in the earlier studies is consistent with a lower capacity for *N*-[^{3}H]methylscopolamine. In each case, however, the fraction of sites ostensibly of low affinity for the unlabeled ligand (i.e. 0.15 to 0.26) represented only 52–58% of the shortfall in relative capacity for *N*-[^{3}H]methylscopolamine and [^{3}H]quinuclidinylbenzilate (i.e. 0.29 to 0.45). This discrepancy has been noted previously [17,19], and the pattern resembles that described here: namely, a subpopulation of sites exhibiting high affinity for unlabeled *N*-methylscopolamine and anomalously low affinity for the radiolabeled analogue. Since the affinities of both *N*-methylscopolamine and scopolamine were measured in each case, using [^{3}H]quinuclidinylbenzilate as the radioligand [17,23,25], Eq. 6 can be used to calculate the amount of contaminating scopolamine that would be required to account for the anomaly between labeled and unlabeled *N*-methylscopolamine. The resulting value of f_2 varies from 0.52 to 2.2, which is comparable to the levels of impurity found in the present investigation. It therefore seems likely that the apparent difference in capacity arose, at least in part, from contaminating scopolamine and its effect on the specific activity of the radioligand.

With radiolabeled agonists, in contrast to antagonists, a shortfall in the apparent capacity is generally characteristic of muscarinic and other G protein-linked receptors. Estimates of maximal binding obtained with [^{3}H]acetylcholine, *cis*-[^{3}H]methyldioxolane, [^{3}H]methylfurmethide, and [^{3}H]oxotremorine-M range from 15 to 75% of those obtained with [^{3}H]quinuclidinylbenzilate, *N*-[^{3}H]methylscopolamine, or *N*-[^{3}H]methyl-4-piperidylbenzilate in membranes from mammalian brain and heart [58–61]. Similarly, maximal binding has been found to vary 7-fold among different radiolabeled agonists in membranes from rat cortex [58]. A subpopulation of high-affinity sites for agonists is expected, however, given the multiphasic inhibitory behavior typically observed in assays with a radiolabeled antagonist. Also, their sensitivity to guanyl nucleotides and their relationship to efficacy attest to their functional importance (see Refs. 10 and 62, and references cited therein). Finally, it has been demonstrated that labeled and unlabeled agonists yield results that are mutually consistent in terms of Scheme 1 (i.e. Eq. 3) (e.g. Ref. 58), in contrast to the pattern obtained with *N*-methylscopolamine (Table 3). The low capacity for radiolabeled agonists therefore appears to be largely a property of the receptor, although a chemical impurity may have been a contributing factor in some cases.

Muscarinic and other G protein-linked receptors are known to occur as homooligomers (e.g. Refs. 7, 63, and 64, and references therein). Such structures raise the possibility that the difference in capacity for *N*-[^{3}H]methylscopolamine and [^{3}H]quinuclidinylbenzilate is a consequence of intermolecular interactions. If the oligomeric status of the cluster is retained under the conditions of the binding assays, the observed heterogeneity could arise from cooperative effects or asymmetry. In an oligomer of otherwise identical monomers, the former is induced by the ligand while the latter is intrinsic to the oligomer. In both cases, the expression for binding at graded concentrations of the radioligand is an

Adair equation (e.g. Ref. 11), and the models are indistinguishable in the absence of other data.

In a strictly asymmetric system, heterogeneity reflects differences in affinity that emerge when the monomeric units assemble to form the oligomer. If the differences between sites within the cluster are small or negligible for one antagonist and large for another, the apparent capacity for the former could exceed that for the latter at practicable concentrations of radioligand. Since the sites remain mutually independent, an asymmetric oligomer of n subunits can be described in terms of Scheme 1 with the proviso that each class of sites represents the fraction $1/n$ of $[R]_t$. Thus, the lines in Fig. 1 could represent binding to a tetrameric array in which clustering led to anomalously weak affinities at one, two, or three of the four sites within the cluster (curves *b–d*, respectively) (Table 1). Such an arrangement can be ruled out for the present data, regardless of the value of n, since Scheme 1 cannot account simultaneously for the binding of labeled and unlabeled *N*-methylscopolamine (Table 3).

In a strictly cooperative system, a difference in apparent capacity could arise from strong negative cooperativity in the binding of one antagonist but not another. Thus, the lines in Fig. 1 can be calculated according to Scheme 2 with the parametric values listed in Table 1. In the absence of cooperative interactions (i.e. $\log p_j = 0$ for all j), the system behaves as a single and uniform population of mutually independent sites (curve *a*). Maximal binding represents the true capacity, and the microscopic dissociation constant (K_P) is numerically identical to the potency in terms of the Langmuir isotherm (EC_{50}) or to the dissociation constant in terms of Scheme 1 (K_{ij}). In the presence of strongly negative cooperativity (i.e. $\log p_j > 4$), the apparent capacity is reduced to 75, 50, or 25% of the true capacity depending upon the level of occupancy at which the cooperative effect occurs (curves *b–d*). Also, there is a concomitant change in the potency of the radioligand (EC_{50}), from 1 nM (curve *a*) to a minimum of 0.25 nM (i.e. K_P/n) when only one of the four sites is accessible (curve *d*). The latter effect arises from the difference between the microscopic and macroscopic dissociation constants when the effective capacity is reduced by negative cooperativity.

The results in Fig. 1 and Table 1 illustrate that the effect of an impurity on binding to identical and independent sites (Eq. 6) can be indistinguishable from negative homotropic cooperativity between interacting sites. Both schemes predict a concomitant and proportionately equal decrease in apparent capacity and in the value of EC_{50}. In contrast to the notion of dissimilar but independent sites, both schemes also can reconcile the binding of *N*-[^{3}H]methylscopolamine and the inhibitory effect of unlabeled *N*-methylscopolamine on the binding of [^{3}H]quinuclidinylbenzilate, at least under some conditions. Indeed, the data represented in Fig. 4 are described somewhat better by Scheme 2, even without the inclusion of scopolamine, than by Scheme 1 with scopolamine taken into account.[4] The mechanistically consistent result obtained with Scheme 2 is made possible by the cooperative effects that can occur between *N*-methylscopolamine and [^{3}H]quinuclidinylbenzilate at interacting sites. Although the two models are not necessarily equivalent, a definitive choice of one over the other is likely to require independent data.

Cooperativity can account for various effects that have emerged in the binding properties of G protein-linked receptors and resist explanation in other terms (e.g. Refs. 7, 10, 62, and 65–69). Moreover, the possibility of cooperative interactions has implications for the mechanism of signalling and suggests a functional role for the oligomers that appear to be a common feature of receptors in G protein-mediated systems [10,14]. Past evidence for cooperativity among muscarinic receptors has included the inhibitory effect of *N*-methylscopolamine at sites apparently labeled only by [^{3}H]quinuclidinylbenzilate [7]. The effect can occur regardless of the relative capacity for *N*-[^{3}H]methylscopolamine and [^{3}H]quinuclidinylbenzilate, which depends upon the conditions and has varied from as low as 0.4 to about 0.75 in previous studies [7,70]. Mass spectra are not available for earlier batches of *N*-[^{3}H]methylscopolamine, but the method of purification was the same for all but the most recent. It therefore seems likely that scopolamine was present at levels comparable to those described here (i.e. $f_i = 0.7–1.2$), and that it was primarily responsible for the shortfall when the relative capacity for *N*-[^{3}H]methylscopolamine and [^{3}H]quinuclidinylbenzilate was about 0.75 or more.

When the relative capacity is lower than about 0.75, the shortfall exceeds the expected effect of scopolamine at known levels of contamination. A relative capacity of 0.5 would require a 9-fold molar excess of scopolamine over *N*-[^{3}H]methylscopolamine (i.e. $f_i = 9.4$), based on the affinities of scopolamine and *N*-methylscopolamine for purified m2 receptors in the present investigation (i.e. Fig. 4: $\log K_{31} = -7.31$, $\log K_{21} = -8.28$). In recent studies on m2 receptors extracted from porcine atria in cholate-NaCl, the apparent capacity for *N*-[^{3}H]methylscopolamine was only 45% of that for [^{3}H]quinuclidinylbenzilate. The batch of *N*-[^{3}H]methylscopolamine used in those experiments was devoid of scopolamine, as indicated by mass spectrometry; in contrast, data analogous to those in Fig. 4B indicate that such a shortfall would require a 10-fold molar excess of scopolamine over *N*-[^{3}H]methylscopolamine.[5] It follows that the larger differences in capacity described previously

[4] In the version of Scheme 2 used for this analysis, binding is expressed as a function of the total concentrations of unlabeled *N*-methylscopolamine, *N*-[^{3}H]methylscopolamine, and [^{3}H]quinuclidinylbenzilate. Contaminating scopolamine was disregarded, but the analysis otherwise was carried out in a mechanistically consistent manner. The formulation of the model has been described previously [7,10].

[5] Park P, Sum CS, Pawagi AB and Wells JW, unpublished observations.

[7,70] arose, in part, from contaminating scopolamine and, in part, from a non-competitive interaction, such as cooperativity. The same effect also may have contributed to the differential capacity in other studies (e.g. Refs. 17, 19, 23, and 25), but an estimate of its magnitude would require data on the levels of contaminating scopolamine. In the case of the present data, shortfalls in the capacity for *N*-[^{3}H]methylscopolamine can be explained wholly in terms of contamination. Cooperative or apparently cooperative effects may have been precluded altogether, for reasons that are unclear, or an intrinsically more complex system may function in a manner superficially consistent with Scheme 1 under some conditions.

Acknowledgments

We are grateful to the managers and staff of Quality Meat Packers Ltd. and the New York Pork and Food Exchange (Toronto) for supplies of porcine atria and for their cooperation in allowing immediate access to fresh tissue. We thank Pauline Bennett, Mario Maniscalco, Steven Souza, and Dr. Ron Vander-Mallie of NEN Life Science Products, Inc. for numerous helpful discussions, for their cooperation in various matters related to the radioligands used in this investigation, including the provision of mass spectra and other information regarding the synthesis, purification, and purity of various products, and for gifts of *N*-[^{3}H]methylscopolamine, *N*-[^{3}H]methylquinuclidinylbenzilate, and [^{3}H]quinuclidinylbenzilate. We also thank Dr. Lingjie Meng of the Molecular Medicine Research Centre and Dr. Jack P. Uetrecht of the Faculty of Pharmacy, University of Toronto, for their advice and assistance regarding the mass spectrometry. Dr. Neil M. Nathanson of the Department of Pharmacology, University of Washington, is thankfully acknowledged for donating the m2-specific antibody 31–1D1 used in the early stages of this investigation. This investigation was supported by the Heart and Stroke Foundation of Ontario (T2970 and T3769) and the Medical Research Council of Canada (MT14171). C.S.S. is the recipient of an Ontario Graduate Fellowship. C.S.S. and N.P. are recipients of Open Fellowships from the School of Graduate Studies, University of Toronto.

Appendix

An unlabeled chemical impurity affects the observed binding of a radioligand in a manner akin to an error in the specific radioactivity. The nature of the effect and its consequences are examined below for Scheme 1, making the assumption that depletion is negligible for all ligands (i.e. $[L_i] \approx [L_i]_t$). A general expression for the binding of a radioligand in a mixture of *m* ligands and *n* classes of sites is given by Eq. 3 in "Materials and methods." For the particular case in which each unlabeled ligand is present at a constant molar ratio with respect to the radioligand (i.e. $f_i = [L_i]/[L_1]$), binding is described by Eq. 5. Taking the value of f_R as 1 and substituting $[R_j]_t$ for $F_j[R]_t$, Eq. 5 can be written alternatively as Eq. A1 or A2 below.

$$\sum_{j=1}^{n}[L_1R_j] = \sum_{j=1}^{n}\frac{[R_j]_t[L_1]}{K_{1j} + [L_1]\left(1+\sum_{i=2}^{m} f_i\frac{K_{1j}}{K_{ij}}\right)} \tag{A1}$$

$$\sum_{j=1}^{n}[L_1R_j] = \sum_{j=1}^{n}\frac{\frac{[R_j]_t}{\left(1+\sum_{i=2}^{m} f_i\frac{K_{1j}}{K_{ij}}\right)}[L_1]}{\frac{K_{1j}}{\left(1+\sum_{i=2}^{m} f_i\frac{K_{1j}}{K_{ij}}\right)} + [L_1]}$$

$$\equiv \sum_{j=1}^{n}\frac{[R_j]_{t,app}[L_1]}{K_{1j,app}+[L_1]} \tag{A2}$$

where

$$[R_j]_{t,app} = \frac{[R_j]_t}{1+\sum_{i=2}^{m} f_i\frac{K_{1j}}{K_{ij}}}, \qquad K_{1j,app} = \frac{K_{1j}}{1+\sum_{i=2}^{m} f_i\frac{K_{1j}}{K_{ij}}}$$

As illustrated by Eq. A2, unidentified or disregarded impurities cause the capacity and the dissociation constant of the radioligand to be underestimated by the factor $1/(1+\Sigma_{i=2}^{m} f_i K_{1j}/K_{ij})$ at each class of sites (cf. Eq. 4 in Ref. 4). Since there is no change in the functional form of the expression, which remains a sum of hyperbolic terms with respect to $[L_1]$, the contamination is undetectable in the absence of other data. The effect of unlabeled impurities is equivalent to an error in the specific activity. If the specific activity of the radioligand *per se* is taken as that stated by the manufacturer (*SA*, Ci/mmol), the effective specific activity of the mixture is given by the expression $SA' = SA/(1+\Sigma_{i=2}^{m} f_i K_{1j}/K_{ij})$. The molar concentration of the radioligand is calculated from the absolute count rate (CR, dpm/mL) according to Eq. A3 or A4; thus, impurities act to increase the effective concentration ($[L_1]'$) as shown in Eq. A5.

$$[L_1] = \frac{CR}{SA \times 2.22 \times 10^{12}} \tag{A3}$$

$$[L_1]' = \frac{CR}{SA' \times 2.22 \times 10^{12}}$$

$$\equiv \frac{CR}{\frac{SA}{1+\sum_{i=2}^{m} f_i\frac{K_{1j}}{K_{ij}}} \times 2.22 \times 10^{12}} \tag{A4}$$

$$[L_1]' = [L_1]\left(1+\sum_{i=2}^{m} f_i\frac{K_{1j}}{K_{ij}}\right) \tag{A5}$$

If the data were analyzed with respect to $[L_1]'$ rather than $[L_1]$, the implicit introduction of the factor $1+\Sigma_{i=2}^{m} f_i K_{1j}/K_{ij}$ would avoid the artifactually low values of $K_{1j,app}$ and $[R_j]_{t,app}$ that otherwise are obtained.

It is noteworthy that even saturating concentrations of the probe fail to yield an estimate of the true capacity. When the concentration of each L_i is a constant fraction of the concentration of the radioligand (i.e. $[L_i] = f_i [L_1]$), the number of sites occupied by the radioligand (i.e. $[L_1R_j]$) is a constant fraction of the total number of occupied sites (i.e. $\Sigma_{i=1}^{m}[L_iR_j]$) for each class of receptor. This is demonstrated in Eqs. A6–A8, which pertain to all concentrations of all ligands provided that depletion is negligible.

For any one class of receptor in Eq. 3 (R_j), the fractional occupancy by the radioligand (L_1) is given by Eq. A6.

$$\frac{[L_1R_j]}{[R_j]_t} = \frac{\dfrac{[L_1]}{K_{1j}}}{1 + \displaystyle\sum_{i=1}^{m} \frac{[L_i]}{K_{ij}}} \tag{A6}$$

An expression analogous to Eq. A6 can be obtained for each ligand present, and the fractional occupancy of R_j by all ligands is given by the sum $\Sigma_{i=1}^{m}[L_iR_j]/[R_j]_t$. Dividing the expression for $[L_1R_j]/[R_j]_t$ (Eq. A6) by the expression for $\Sigma_{i=1}^{m}[L_iR_j]/[R_j]_t$ yields the occupancy of R_j by L_1 relative to the total occupancy by all ligands, as shown in Eq. A7.

$$\frac{[L_1R_j]}{\displaystyle\sum_{i=1}^{m}[L_iR_j]} = \frac{\dfrac{[L_1]}{K_{1j}}}{\displaystyle\sum_{i=1}^{m}\frac{[L_i]}{K_{ij}}} \tag{A7}$$

Since $[L_i]$ is a constant fraction of $[L_1]$ for each ligand i (i.e. $[L_i] = f_i[L_1]$), each term in the denominator of Eq. A7 can be expressed in terms of $[L_1]$ and then simplified as in Eq. A8.

$$\frac{[L_1R_j]}{\displaystyle\sum_{i=1}^{m}[L_iR_j]} = \frac{\dfrac{[L_1]}{K_{1j}}}{\dfrac{[L_1]}{K_{1j}} + \displaystyle\sum_{i=2}^{m} f_i \frac{[L_1]}{K_{ij}}}$$

$$\equiv \frac{\dfrac{1}{K_{1j}}}{\dfrac{1}{K_{1j}} + \displaystyle\sum_{i=2}^{m}\frac{f_i}{K_{ij}}} \tag{A8}$$

As illustrated by the last term of Eq. A8, the ratio of labeled receptor to all liganded receptor depends only upon the values of the constants f_i and K_{ij}. That ratio, therefore, is independent of the concentrations of all ligands, and the apparent capacity ($[R_j]_{t,app}$) differs from the true capacity ($[R_j]_t$) by the factor $1/(1+\Sigma_{i=2}^{m} f_i K_{1j}/K_{ij})$ as shown in Eq. A2.

Equations A1–A2 and A6–A8 are helpful for illustrative purposes, but they are inappropriate if binding reduces the free concentration of one or more ligands. Strictly speaking, the value of f_i is a constant only when defined as the ratio of the total concentrations of unlabeled and labeled ligands. Since the dose-dependence of depletion will differ for ligands of different affinity, the corresponding values of f_i in Eqs. A1–A8 will vary with the concentration of L_1. Such variations in f_i may affect the fitted estimates of parametric values and lead to divergence between the data and an otherwise appropriate model. Depletion becomes progressively less as the receptor becomes saturated, however, and Eq. A8 becomes increasingly accurate at higher concentrations of ligand. It therefore seems likely that depletion will have little effect on the apparent capacity (e.g. $[R_j]_{t,app}$ in Eq. A2), since estimates of maximal binding are determined primarily by the data at the highest concentrations of the radioligand. Except in extreme cases, when the free concentration of a ligand becomes very small, problems associated with the mutual depletion of receptor and ligand are avoided altogether by formulating the model in terms of total concentrations and defining f_i accordingly.

A special case arises when the probe and an unlabeled ligand are of equal affinity for each R_j. If K_{1j} equals K_{2j}, for example, Eq. A2 can be written as Eq. A9. The corresponding expression with only two ligands is shown as Eq. A10.

$$\sum_{j=1}^{n}[L_1R_j] = \sum_{j=1}^{n} \frac{\dfrac{[R_j]_t}{\left(1 + f_2 + \displaystyle\sum_{i=3}^{m} f_i \frac{K_{1j}}{K_{ij}}\right)}[L_1]}{\dfrac{K_{1j}}{\left(1 + f_2 + \displaystyle\sum_{i=3}^{m} f_i \frac{K_{1j}}{K_{ij}}\right)} + [L_1]} \tag{A9}$$

$$\sum_{j=1}^{n}[L_1R_j] = \sum_{j=1}^{n} \frac{\dfrac{[R_j]_t}{(1+f_2)}[L_1]}{\dfrac{K_{1j}}{(1+f_2)} + [L_1]} \tag{A10}$$

The situation described by Eq. A10 typically is encountered when L_1 and L_2 represent the tritiated and unlabeled analogues of the same ligand. In such a case, the specific radioactivity quoted by the manufacturer generally would have been reduced by the factor $1/(1+f_2)$ from that of an isotopically pure product. The quantity $1+f_2$ therefore is implicit in the concentration of L_1 as calculated from the rate of isotopic decay. That, in turn, compensates for the effect that the unlabeled ligand otherwise would have on B_{max} and EC_{50}. A practical advantage of Eq. A10 relates to the disappearance of K_1/K_2, which is assumed to equal 1. The adjusted value of the specific activity is therefore a constant provided that the labeled and unlabeled ligands have the same affinity for the receptor.

Equation A10 admits only one radiolabeled species and, therefore, is simplistic for many applications. Tritium gen-

erally is incorporated at two or more positions on the parent compound. Since the complete exclusion of hydrogen is unlikely, most products contain a mixture of labeled species that supposedly are of equal affinity for the receptor; for example, a ligand formed by methylation of a tertiary amine has four possible arrangements: $^{3}H_3C$-R (L_1), $^{3}H_2{}^{1}H_1C$-R (L_2), $^{3}H_1{}^{1}H_2C$-R (L_3), and $^{1}H_3C$-R (L_4). Binding in terms of Scheme 1, therefore, is described by Eq. A11 ($m = 4$, $f_i = [L_i]/[L_1]$), where the specific activity of the mixture can be calculated from the quantity $1 + f_2 + f_3 + f_4$ and the number of β-emitting atoms per methyl group.

$$\sum_{j=1}^{n}([L_1R_j] + [L_2R_j] + [L_3R_j]) = \sum_{j=1}^{n} \frac{\dfrac{[R_j]_t\,(1 + f_2 + f_3)}{(1 + f_2 + f_3 + f_4)}[L_1]}{\dfrac{K_{1j}}{(1 + f_2 + f_3 + f_4)} + [L_1]} \quad \text{(A11)}$$

The expressions presented above illustrate how chemically distinct impurities and the protonated analogue of a tritiated radioligand are essentially the same in their effects on binding. The functional form of the binding isotherm is the same throughout, and the effect of the unlabeled ligand can be accommodated in the value of the specific activity. Protonated analogues of tritiated ligands generally are identified in the mass spectrum, and the specific activity is adjusted accordingly by the manufacturer. A similar adjustment is possible for chemically distinct impurities, but the corrected value is sensitive to changes in the relative affinity of the contaminant and the radioligand. The effect of a non-emitting or transparent contaminant on the apparent specific signal of a probe is a problem of general importance. Expressions analogous to those described above can be formulated for compounds tagged with spin labels or fluorescent groups.

The prevalence of unlabeled chemical impurities in radioligands from commercial sources is largely unknown, and their effects can be difficult to recognize or to distinguish from other phenomena. It follows that any conclusion based on the specific activity ought to be viewed with caution, at least until the purity of the product is confirmed. With any radioligand, a minimum precaution would be to inspect the mass spectrum of each batch. If a local mass spectrometer is not equipped to handle radionuclides, the data may be available from the manufacturer. Indeed, it would be helpful if the spectrum were supplied with the product on a routine basis. Impurities also can be detected by chromatographic procedures, although the amounts required may be prohibitively large for routine sampling; also, facilities for radionuclides may not be readily available. Potential contaminants sometimes can be identified from a knowledge of the synthetic pathway and examined independently for their affinity for the receptor, as in the present example of scopolamine and *N*-[^{3}H]methylscopolamine. If the relative affinity of the radioligand and the impurity is unfavorable, as in the case of *N*-[^{3}H]methylquinuclidinylbenzilate and quinuclidinylbenzilate, even minor amounts of the latter will interfere in the binding assays. A sufficiently unfavorable ratio may preclude adequate levels of purity, at least on a routine basis, and render the radioligand almost useless for quantitative work. The clear preference is to avoid impurities altogether by selecting an appropriate synthetic pathway and by optimizing the conditions of synthesis and purification. If impurities cannot be avoided, a practical recourse may be to adjust the nominal specific activity by comparing each batch of the product with a standard of confirmed purity.

References

[1] Boeynaems JM, Dumont JE. Quantitative analysis of the binding of ligands to their receptors. J Cyclic Nucleotide Res 1975;1:123–42.

[2] Reimann EM, Soloff MS. The effect of radioactive contaminants on the estimation of binding parameters by Scatchard analysis. Biochim Biophys Acta 1978;533:130–9.

[3] Munson PJ. Experimental artifacts and the analysis of ligand binding data: results of a computer simulation. J Recept Res 1983;3:249–59.

[4] Lazareno S, Birdsall NJM. Effects of contamination on radioligand binding parameters. Trends Pharmacol Sci 2000;21:57–60.

[5] Rovati GE. The many faces of binding artefacts. Trends Pharmacol Sci 2000;21:168–9.

[6] Sum CS, Pyo N, Wells JW. Effects of chemical impurities on the binding of radioligands, illustrated with cardiac muscarinic receptors. Soc Neurosci Abstr 2000;26:1912.

[7] Wreggett KA, Wells JW. Cooperativity manifest in the binding properties of purified cardiac muscarinic receptors. J Biol Chem 1995; 270:22488–99.

[8] Peterson GL, Schimerlik MI. Large scale preparation and characterization of membrane-bound and detergent-solubilized muscarinic acetylcholine receptor from pig atria. Prep Biochem 1984;14:33–47.

[9] Wong H-MS, Sole MJ, Wells JW. Assessment of mechanistic proposals for the binding of agonists to cardiac muscarinic receptors. Biochemistry 1986;25:6995–7008.

[10] Chidiac P, Green MA, Pawagi AB, Wells JW. Cardiac muscarinic receptors. Cooperativity as the basis for multiple states of affinity. Biochemistry 1997;36:7361–79.

[11] Wells JW. Analysis and interpretation of binding at equilibrium. In: Hulme EC, editor. Receptor-ligand interactions: a practical approach. Oxford: Oxford University Press, 1992. p. 289–395.

[12] Seeman P, Ulpian C, Wreggett KA, Wells JW. Dopamine receptor parameters detected by [^{3}H]spiperone depend on tissue concentration: analysis and examples. J Neurochem 1984;43:221–35.

[13] Marquardt DW. An algorithm for least-squares estimation of nonlinear parameters. J Soc Indust Appl Math 1963;2:431–41.

[14] Chidiac P, Wells JW. Effects of adenyl nucleotides and carbachol on cooperative interactions among G proteins. Biochemistry 1992;31: 10908–21.

[15] Sum CS, Wells JW. Co-operative potential of M_2 muscarinic receptors. Life Sci 1999;64:558.

[16] Brown JH, Goldstein D, Masters SB. The putative M_1 muscarinic receptor does not regulate phosphoinositide hydrolysis. Studies with pirenzepine and McN-A343 in chick heart and astrocytoma cells. Mol Pharmacol 1985;27:525–31.

[17] Brown JH, Goldstein D. Analysis of cardiac muscarinic receptors recognized selectively by nonquaternary but not by quaternary ligands. J Pharmacol Exp Ther 1986;238:580–6.

[18] Gibson RE, Rzeszotarski WJ, Jagoda EM, Francis BE, Reba RC, Eckelman WC. [^{125}I]3-Quinuclidinyl 4-iodobenzilate: a high affinity, high specific activity radioligand for the M_1, and M_2-acetylcholine receptors. Life Sci 1984;34:2287–96.
[19] El-Fakahany EE, Ramkumar V, Lai WS. Multiple binding affinities of *N*-methylscopolamine to brain muscarinic acetylcholine receptors: differentiation from M_1 and M_2 receptor subtypes. J Pharmacol Exp Ther 1986;238:554–63.
[20] Yang CM, Yeh H-M, Sung T-C, Chen F-F, Wang Y-Y. Characterization of muscarinic receptor subtypes in canine left ventricular membranes. J Recept Res 1992;12:427–49.
[21] Masters SB, Quinn MT, Brown JH. Agonist-induced desensitization of muscarinic receptor-mediated calcium efflux without concomitant desensitization of phosphoinositide hydrolysis. Mol Pharmacol 1985; 27:325–32.
[22] Evans T, Smith MM, Tanner LI, Harden TK. Muscarinic cholinergic receptors of two cell lines that regulate cyclic AMP metabolism by different molecular mechanisms. Mol Pharmacol 1984;26:395–404.
[23] Lee JH, El-Fakahany EE. Heterogeneity of binding of muscarinic receptor antagonists in rat brain homogenates. J Pharmacol Exp Ther 1985;233:707–14.
[24] Lee NH, Ramkumar V, El-Fakahany EE. Charge but not chemical class explains the selective binding of *N*-[^{3}H]methylscopolamine to a subpopulation of [^{3}H]quinuclidinylbenzilate binding sites in rat cerebral cortex homogenates. Eur J Pharmacol 1986;130:153–5.
[25] Norman AB, Eubanks JH, Creese I. Irreversible and quaternary muscarinic antagonists discriminate multiple muscarinic receptor binding sites in rat brain. J Pharmacol Exp Ther 1989;248:1116–22.
[26] Galper JB, Dziekan LC, O'Hara DS, Smith TW. The biphasic response of muscarinic cholinergic receptors in cultured heart cells to agonists. Effects on receptor number and affinity in intact cells and homogenates. J Biol Chem 1982;257:10344–56.
[27] van Koppen CJ, Nathanson NM. Site-directed mutagenesis of the m2 muscarinic acetylcholine receptor. Analysis of the role of *N*-glycosylation in receptor expression and function. J Biol Chem 1990;265: 20887–92.
[28] Hulme EC, Birdsall NJM, Burgen ASV, Mehta P. The binding of antagonists to brain muscarinic receptors. Mol Pharmacol 1978;14: 737–50.
[29] Fisher SK. Recognition of muscarinic cholinergic receptors in human SK-N-SH neuroblastoma cells by quaternary and tertiary ligands is dependent upon temperature, cell integrity, and the presence of agonists. Mol Pharmacol 1988;33:414–22.
[30] Harden TK, Petch LA, Traynelis SF, Waldo GL. Agonist-induced alteration in the membrane form of muscarinic cholinergic receptors. J Biol Chem 1985;260:13060–6.
[31] Castoldi AF, Fitzgerald B, Manzo L, Tonini M, Costa LG. Muscarinic M_2 receptors in rat brain labeled with [^{3}H]AF-DX 384. Res Commun Chem Pathol Pharmacol 1991;74:371–4.
[32] Entzeroth M, Mayer N. The binding of [^{3}H]AF-DX 384 to rat ileal smooth muscle muscarinic receptors. J Recept Res 1991;11:141–52.
[33] Bonner TI, Buckley NJ, Young AC, Brann MR. Identification of a family of muscarinic acetylcholine receptor genes. Science 1987;237: 527–32.
[34] Bonner TI, Young AC, Brann MR, Buckley NJ. Cloning and expression of the human and rat m5 muscarinic acetylcholine receptor genes. Neuron 1988;1:403–10.
[35] Buckley NJ, Bonner TI, Buckley CM, Brann MR. Antagonist binding properties of five cloned muscarinic receptors expressed in CHO-K1 cells. Mol Pharmacol 1989;35:469–76.
[36] Dörje F, Wess J, Lambrecht G, Tacke R, Mutschler E, Brann MR. Antagonist binding profiles of five cloned human muscarinic receptor subtypes. J Pharmacol Exp Ther 1991;256:727–33.
[37] Rinken A, Kameyama K, Haga T, Engström L. Solubilization of muscarinic receptor subtypes from baculovirus infected *Sf*9 insect cells. Biochem Pharmacol 1994;48:1245–51.
[38] Dong GZ, Kameyama K, Rinken A, Haga T. Ligand binding properties of muscarinic acetylcholine receptor subtypes (m1–m5) expressed in baculovirus-infected insect cells. J Pharmacol Exp Ther 1995;274:378–84.
[39] Hammer R, Berrie CP, Birdsall NJM, Burgen ASV, Hulme EC. Pirenzepine distinguishes between different subclasses of muscarinic receptors. Nature 1980;283:90–2.
[40] Hulme EC, Birdsall NJM, Buckley NJ. Muscarinic receptor subtypes. Annu Rev Pharmacol Toxicol 1990;30:633–73.
[41] Lazareno S, Buckley NJ, Roberts FF. Characterization of muscarinic M_4 binding sites in rabbit lung, chicken heart, and NG108–15 cells. Mol Pharmacol 1990;38:805–15.
[42] Tietje KM, Goldman PS, Nathanson NM. Cloning and functional analysis of a gene encoding a novel muscarinic acetylcholine receptor expressed in chick heart and brain. J Biol Chem 1990;265:2828–34.
[43] Sharma VK, Colecraft HM, Rubin LE, Sheu SS. Does mammalian heart contain only the M_2 muscarinic receptor subtype? Life Sci 1997;60:1023–9.
[44] Luetje CW, Brumwell C, Norman MG, Peterson GL, Schimerlik MI, Nathanson NM. Isolation and characterization of monoclonal antibodies specific for the cardiac muscarinic acetylcholine receptor. Biochemistry 1987;26:6892–6.
[45] Maeda A, Kubo T, Mishina M, Numa S. Tissue distribution of mRNAs encoding muscarinic acetylcholine receptor subtypes. FEBS Lett 1988;239:339–42.
[46] Lameh J, Philip M, Sharma YK, Moro O, Ramachandran J, Sadée W. Hm1 muscarinic cholinergic receptor internalization requires a domain in the third cytoplasmic loop. J Biol Chem 1992;267:13406–12.
[47] Moro O, Lameh J, Sadée W. Serine- and threonine-rich domain regulates internalization of muscarinic cholinergic receptors. J Biol Chem 1993;268:6862–5.
[48] Tsuga H, Kameyama K, Haga T, Kurose H, Nagao T. Sequestration of muscarinic acetylcholine receptor m2 subtypes. Facilitation by G protein-coupled receptor kinase (GRK2) and attenuation by a dominant-negative mutant of GRK2. J Biol Chem 1994;269:32522–7.
[49] Pals-Rylaarsdam R, Xu Y, Witt-Enderby P, Benovic JL, Hosey MM. Desensitization and internalization of the m2 muscarinic acetylcholine receptor are directed by independent mechanisms. J Biol Chem 1995;270:29004–11.
[50] Pals-Rylaarsdam R, Hosey MM. Two homologous phosphorylation domains differentially contribute to desensitization and internalization of the m2 muscarinic acetylcholine receptor. J Biol Chem 1997; 272:14152–8.
[51] Shockley MS, Burford NT, Sadée W, Lameh J. Residues specifically involved in down-regulation but not internalization of the m1 muscarinic acetylcholine receptor. J Neurochem 1997;68:601–9.
[52] Tsuga H, Kameyama K, Haga T, Honma T, Lameh J, Sadée W. Internalization and down- regulation of human muscarinic acetylcholine receptor m2 subtypes. Role of third intracellular m2 loop and G protein-coupled receptor kinase 2. J Biol Chem 1998;273:5323–30.
[53] Vögler O, Bogatkewitsch GS, Wriske C, Krummenerl P, Jakobs KH, van Koppen CJ. Receptor subtype-specific regulation of muscarinic acetylcholine receptor sequestration by dynamin. Distinct sequestration of m2 receptors. J Biol Chem 1998;273:12155–60.
[54] Roseberry AG, Hosey MM. Trafficking of M_2 muscarinic acetylcholine receptors. J Biol Chem 1999;274:33671–6.
[55] Shockley MS, Tolbert LM, Tobin AB, Nahorski SR, Sadee W, Lameh J. Differential regulation of muscarinic M_1 and M_3 receptors by a putative phosphorylation domain. Eur J Pharmacol 1999;377:137–46.
[56] Tolbert LM, Lameh J. Human muscarinic cholinergic receptor Hm1 internalizes via clathrin-coated vesicles. J Biol Chem 1996;271: 17335–42.
[57] Lee KB, Pals-Rylaarsdam R, Benovic JL, Hosey MM. Arrestin-independent internalization of the m1, m3, and m4 subtypes of muscarinic cholinergic receptors. J Biol Chem 1998;273:12967–72.
[58] Birdsall NJM, Burgen ASV, Hulme EC. The binding of agonists to brain muscarinic receptors. Mol Pharmacol 1978;14:723–36.

[59] Harden TK, Meeker RB, Martin MW. Interaction of a radiolabeled agonist with cardiac muscarinic cholinergic receptors. J Pharmacol Exp Ther 1983;227:570–7.
[60] Gurwitz D, Kloog Y, Sokolovsky M. High affinity binding of [^{3}H]acetylcholine to muscarinic receptors. Regional distribution and modulation by guanine nucleotides. Mol Pharmacol 1985;28:297–305.
[61] Gillard M, Waelbroeck M, Christophe J. Muscarinic receptor heterogeneity in rat central nervous system. II. Brain receptors labeled by [^{3}H]oxotremorine-M correspond to heterogeneous M2 receptors with very high affinity for agonists. Mol Pharmacol 1987;32:100–8.
[62] Green MA, Chidiac P, Wells JW. Cardiac muscarinic receptors: relationship between the G protein and multiple states of affinity. Biochemistry 1997;36:7380–94.
[63] Hébert TE, Bouvier M. Structural and functional aspects of G protein-coupled receptor oligomerization. Biochem Cell Biol 1998;76:1–11.
[64] Zeng F-Y, Wess J. Identification and molecular characterization of m3 muscarinic receptor dimers. J Biol Chem 1999;274:19487–97.
[65] Henis YI, Sokolovsky M. Muscarinic antagonists induce different receptor conformations in rat adenohypophysis. Mol Pharmacol 1983;24:357–65.
[66] Mattera R, Pitts BJ, Entman ML, Birnbaumer L. Guanine nucleotide regulation of a mammalian myocardial muscarinic receptor system. Evidence for homo- and heterotropic cooperativity in ligand binding analyzed by computer-assisted curve fitting. J Biol Chem 1985;260:7410–21.
[67] Boyer JL, Martínez-Cárcamo M, Monroy-Sánchez JA, Posadas C, García-Sáinz JA. Guanine nucleotide-induced positive cooperativity in muscarinic-cholinergic antagonist binding. Biochem Biophys Res Commun 1986;134:172–7.
[68] Sinkins WG, Wells JW. G protein-linked receptors labeled by [^{3}H]histamine in guinea pig cerebral cortex. II, Mechanistic basis for multiple states of affinity. Mol Pharmacol 1993;43:583–94.
[69] Jordan BA, Devi LA. G-protein-coupled receptor heterodimerization modulates receptor function. Nature 1999;399:697–700.
[70] Pawagi AB, Pyo N, Park P, Sum CS, Wells JW. Latent cardiac muscarinic receptors. Soc Neurosci Abstr 1999;25:1726.